Influence of Strain Rate Sensitivity on Cube Texture Evolution in Aluminium Alloys

ELISA CANTERGIANI, GEORG FALKINGER, STEFAN MITSCHE, MORITZ THEISSING, SILKE KLITSCHKE, and FRANZ ROTERS

The influence of strain rate sensitivity on development of Cube texture and on the morphology of Cube-oriented grains is often neglected in simulations approaches. Therefore, crystal plasticity simulations and experiments were performed up to 73 pct of thickness reduction for cold rolling on Al 6016. It is found, that low values of strain rate sensitivity promote Cube grains fragmentation and avoid formation of transition bands already at 50 to 55 pct thickness reduction. High values of strain-rate sensitivity cause formation of Cube transition bands leaving thin Cube grains in the microstructure and delay their fragmentation. Other texture components are affected by changes in strain rate sensitivity as well. The Copper volume fraction in the final texture diminishes as the strain rate sensitivity decreases, while Brass and S components of the beta fiber show a moderately higher volume fraction when the strain rate sensitivity increases. The final volume fraction of Goss is highest when the strain rate sensitivity is 10^{-2} but low if the strain rate sensitivity is 10^{-3} or raises up to 10^{-1}. Recrystallization texture components (P, Q) are not affected by strain rate sensitivity, while the invGoss fraction decreases for high values of strain rate sensitivity. The results found in cold rolling crystal plasticity simulations were compared with experimentally determined Cube distribution and texture components obtained through thickness for Al6016 rolled at 80 m/min and 600 m/min. Further crystal plasticity simulations were performed to predict the influence of strain rate sensitivity during several hot rolling conditions where activity of non-octahedral slip systems was included in the simulations. During hot rolling, high values of strain rate sensitivity contribute to Cube stabilization and promote formation of Copper texture and delay Brass and S.

I. INTRODUCTION

CUBE texture evolution in aluminium alloys is considered with special attention because of its preferential growth during the recrystallization heat treatment of cold rolled aluminium sheets causing anisotropy responsible for forming defects during deep-drawing. The strain rate sensitivity (m) is a material parameter describing the variation of flow stress under a change of strain rate and it depends both on temperature and strain rate of deformation. According to Chapuis et al.[1] the value of strain rate sensitivity for an alloy depends both on extrinsic effects (e.g. temperature and strain rate) and intrinsic effects (e.g. grain size and alloy composition). Depending on composition and heat treatment history, during cold deformation, aluminium alloys can exhibit positive or negative strain rate sensitivity depending on strain rate. During hot deformation, when thermal activation of dislocation glide becomes important, the flow stress of the material is both temperature and strain rate dependent and for several metals, the strain rate sensitivity increases as the deformation temperature approaches the melting temperature.[2] During forming, a positive value of m is beneficial to delay strain localization, on the contrary, a negative value will localize early plastic flow. Positive values of strain rate sensitivity as function of strain rate from 10^{-4} s^{-1} to 1 s^{-1} were measured for aluminium alloys AA1200 and AA3103,[3] while negative values of m in Al–Mg alloys at room temperature are attributed

ELISA CANTERGIANI and FRANZ ROTERS are with the Max-Planck-Institut für Eisenforschung, Max-Planck-Straβe 1, 40237 Düsseldorf, Germany. Contact e-mails: e.cantergiani@mpie.de, f.roters@mpie.de. GEORG FALKINGER is with the AMAG Rolling GmbH, 5282 Ranshofen, Austria. STEFAN MITSCHE and MORITZ THEISSING are with the Institute of Electron Microscopy and Nanoanalysis and Center for Electron Microscopy, Graz University of Technology, NAWI Graz, Steyrergasse 17, 8010 Graz, Austria. SILKE KLITSCHKE is with the Fraunhofer-Institut for Mechanics of Materials IWM, Wöhlerstraβe 11, 79108 Freiburg, Germany.

to dynamic strain ageing caused by interaction of Mg atoms with dislocations.[4] The strain rate sensitivity value for Al–Mg alloys in uniaxial tension was found to increase up to 0.4 at a temperature of 300 °C.[5] For the 7056 alloy, the increase of m as function of temperature for compression loads depends on the temper state of the alloy.[6] For other aluminium alloys, the strain rate sensitivity was found to increase with augmentation of dislocation density and thus of plastic strain.[7] Ultra-fine grain aluminium alloys have high strain rate sensitivity even at low strain rates because of grain boundary sliding compared to coarse-grained alloys.[7] Other studies compared the strain rate sensitivity of conventional grain sized and ultra-fine grain sized Al 6061 as function of temperature and proved that strain rate sensitivity increases as temperature rises but this dependence is more pronounced for ultra-fine grain alloys.[8] Strain rate sensitivity values for Al–Mg alloys containing different amounts of manganese or scandium were measured as function of temperature with values ranging from 0.02 at room temperature up to 0.20, 0.30, or 0.42 depending on alloy composition.[9] Table I shows a summary of some experimentally determined strain rate sensitivity values for several aluminium alloys. The influence of different strain rates on texture evolution during cold rolling was assessed on brass containing 5 wt pct of zinc showing that low strain rates produce a Copper texture while high strain rates move texture to Brass orientation.[10] The dependence of texture on strain rate in FCC metals is attributed to the activation energy required for cross-slip which is dependent both on temperature and strain rate.[10] For brass containing zinc, a Copper dominated texture is developed when extensive cross slip occurs on octahedral slip systems, while the texture is Brass dominated when slip occurs on octahedral slip systems without extensive cross-slip.[11]

In texture simulations, the influence of strain rate sensitivity of aluminium alloys was investigated through Taylor type models using relaxed constraints (RC) where the standard Taylor equation describing the strain rate tensor was modified to account for strain rate sensitivity (m).[12] The strain rate sensitivity values used in these simulations were 0.05 for room temperature deformation, 0.15 for deformation at intermediate temperatures and 0.25 for temperatures exceeding 500 °C. In the same study, values for strain rate sensitivity at different temperatures were measured for the 8090 Al–Li alloy and m was found to be 0.003 at room temperature and raising to 0.17 at 450 °C.[12] The results of these simulations suggest that high values of strain rate sensitivity are responsible for strong Brass texture, however, the shear ε_{12} was found to be the key contributing factor for the strong Brass texture development in hot rolling. On the contrary, low values of m would favor generation of S orientation instead of Brass.[12] The Needleman and Asaro rate dependent model[13] was used to simulate texture evolution of two different aluminium microstructures (one containing mainly Cube grains and one with random texture) at room temperature and at 375 °C followed by a comparison with plane strain compression tests; but this model failed to capture Cube stabilization and

strong texture intensity at high temperature and it predicted a large Copper/Brass ratio compared to experiments.[14]

Recently, the influence of strain rate sensitivity was investigated using visco-plastic self-consistent modeling (VPSC), showing that strain rate sensitivity influences the deformation mode activity and thus the strain anisotropy and texture development.[1] VPSC simulations indicate that high values of strain rate sensitivity (m) result in more isotropic deformation and weak texture.[1] VPSC is used to evaluate global texture evolution, however, in this simulation framework, a grain is considered to interact with a surrounding matrix, whose constitutive behavior is an average of the mechanical properties of the polycrystal.[15] As mentioned in literature,[16] crystal plasticity full-field methods are more accurate to predict texture evolution and the real geometry of grains (spatially resolved model) can be used as input.

The strain rate sensitivity is a parameter which is often characterized in fully laminated and aged aluminium alloys before forming operations or during hot rolling through compression tests at different temperatures and strain rates. However, during cold rolling its influence on texture (especially on Cube oriented grains) is still neglected. In literature, there is a lack of experimental evidence of the influence of rolling speed on texture evolution in industrial rolling plants for aluminium alloys. Moreover, previous simulation studies[12,13] failed in predicting texture evolution as function of strain rate sensitivity due to the limitations of the grain interactions representation of these models. Other approaches (VPSC[1]) were not able to capture the dependence of Cube on strain rate sensitivity.

The purpose of the paper is thus to assess the influence of variations of strain rate sensitivity through full field crystal plasticity simulations and through experiments on texture evolution in an aluminium alloy (Al 6016) with attention to the Cube morphology and its volume fraction evolution as function of thickness reduction. Microstructures extracted from electron backscatter diffraction (EBSD) of hot bands with a high number of Cube oriented grains will be used as input in the simulations. Experimental results from cold rolling experiments performed in an industrial rolling plant at two different speeds on Al 6016 are included and compared with simulations. A further assessment of strain rate sensitivity influence on texture development during hot rolling with activation of non-octahedral slip systems is also presented and discussed.

II. COLD ROLLING EXPERIMENTS ON AL 6016

A series of cold-rolling experiments was performed starting from the same hot band of Al 6016 with an initial thickness of 4 mm. Figures 1(a) and (b) show the rolling direction (RD) and the normal direction (ND) inverse pole figure (IPF) colors, respectively for the initial microstructure. Figure 1(c) shows a distribution map of the grains pertaining to Cube orientation colored with different intensity depending on their

Table I. Values of Strain Rate Sensitivity for Aluminium Alloys Tested in Tension (T) or Compression (C) at Room Temperature (RT) or at High Temperature and Several Orders of Strain Rates

| Material	Temp. [°C]	Strain Rate [s^{-1}]	Type of Test (Tension or Compression)	Value or Range of Strain Rate sensitivity (m)	Reference
Al 5083	450	10^{-4} to 10^{-3}	T	0.33	17
Al–Mg 6.8	25 to 300	10^{-4} to 10^{-2}	T	0.15-0.4	5
Al 6016	RT	380 to 1750	T	0.0377	18
Al 5182	RT	370 to 1520	T	0.035	18
AlMgMn alloys	50 to 450	0.1 to 1	T	0.02 to 0.2	9
AlMg3.5Sc0.1	50 to 450	0.1 to 1	T	0.02 to 0.24	9
AlMg4.5Sc0.26	50 to 450	0.02 to 0.44	T	0.02 to 0.44	9
AA 1200	RT	10^{-4} to 1	T	0.0096	3
AA 3103	RT	10^{-4} to 1	T	0.0311	3
AA 6016	RT-510 °C	Not specified	T	0.01 to 0.15	19
Al 6063-T6	RT	0.001 to 850	C	0.0072	20
Al 6082-T6	RT	0.1 to 3000	C	0.008	21
Al 7108-T79	RT	0.1 to 3000	C	0.022	21
Al (99.999 pct single crystal)	RT	0.001 to 1000	C	0.044	22
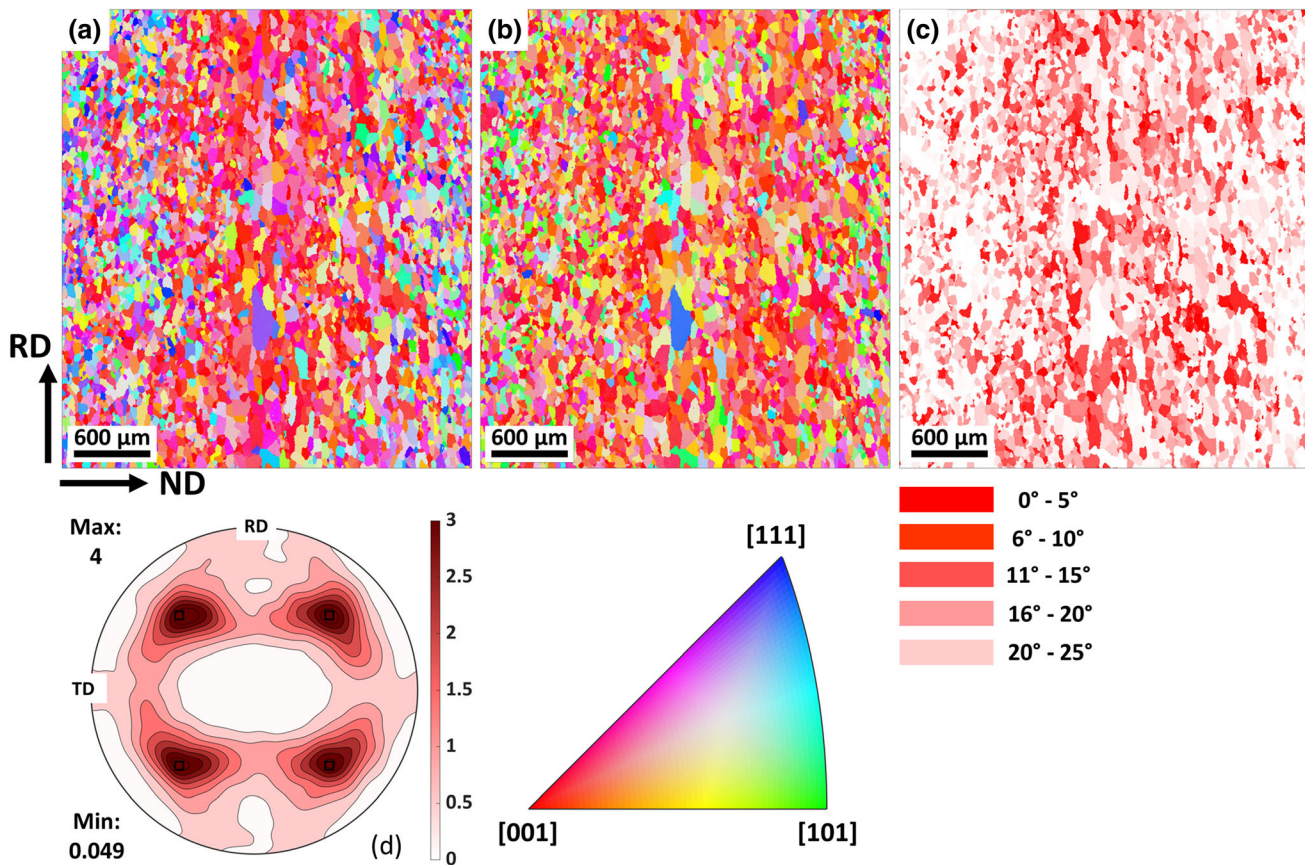
Fig. 1—IPF for rolling direction (RD) (*a*) and IPF for normal direction (ND) (*b*) of the initial RD-ND section for the Al 6016 hot band used for experimental cold rolling tests. The distribution of Cube grains considering max. 25 deg misorientation is shown in (*c*). The Cube texture intensity is shown in the (111) pole figure (*d*).

misorientation (max. up to 25 deg), while Figure 1(d) shows the (111) pole figure where a strong Cube texture is present. The majority of Cube grains is concentrated in the center of the thickness while less Cube grains are found close to the sheet surfaces. The initial hot band texture calculated through harmonic series expansion with a half-width of 5 deg is plotted as sections of the orientation distribution function (ODF) in Figure 2,
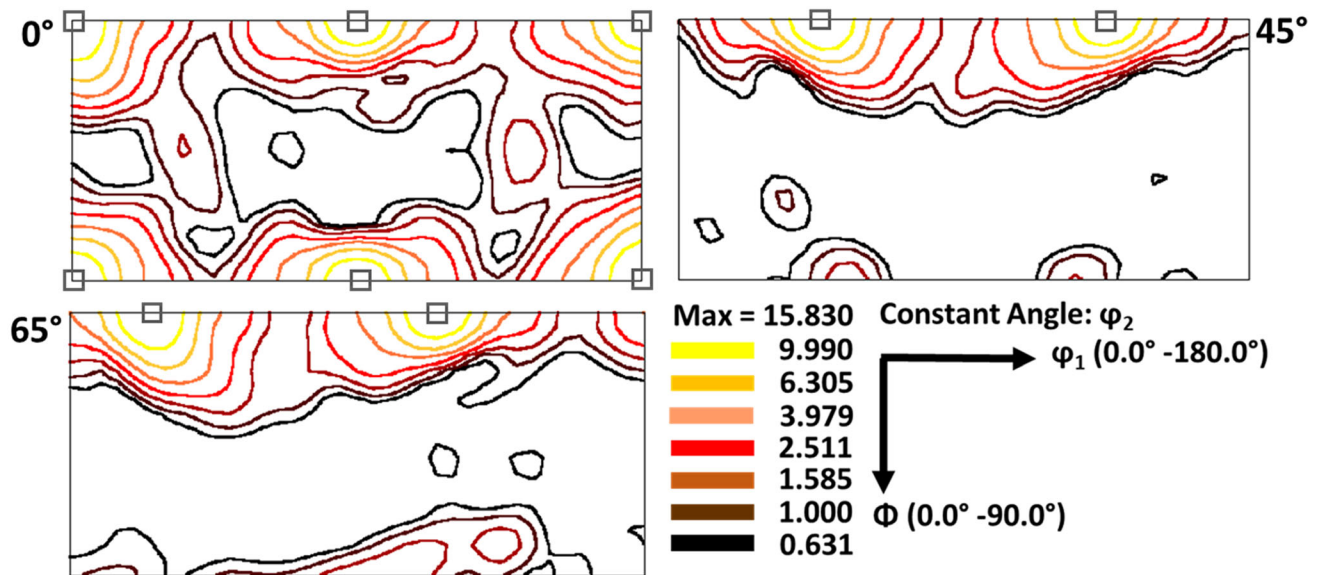
Fig. 2—Orientation distribution function (ODF) sections (0, 45, 65 deg) for the Al 6016 hot band used for cold rolling experiments. Square markers indicate position of the Cube texture component in the ODF sections.

where Cube is the main texture component present in the microstructure. The electron back-scattered diffraction (EBSD) maps were obtained with a scanning electron microscope SEM Zeiss Ultra 55 equipped with a Thorlabs Fast Frame Rate Scientific camera and the collecting Software OIM DC V7.3.1. For the hot band, an RD-ND area of 4000 μm × 4000 μm with a step size of 4 μm was selected, while the step size was reduced to 0.4 μm for areas of 400 μm × 400 μm to obtain higher resolutions scans. Two coils cold rolled at different speed were produced in the industrial cold rolling plant at AMAG Rolling GmbH. One coil was obtained at a speed of 80 m/min and a second coil was fabricated at a speed of 600 m/min. The actual strain rate experienced by the material in both cases is not known, but assuming vanishing tensile stresses in the band and a constant strain rate throughout the roll gap, the two rolling speeds were estimated to correspond to strain rates of 60 and 450 s^{-1} respectively. These strain rates were estimated by multiplying the rolling strain with the rolling speed divided by the contact length between rollers and aluminium sheet. Cold rolled samples were extracted after 55 and 73 pct thickness reduction for both cold rolling speeds and EBSD scans were obtained to calculate texture volume fractions and orientation distribution functions. For the 55 pct cold rolled samples, EBSD scans were taken in a RD-ND section covering an area of 2000 μm × 1700 μm with a step size of 2 μm. At 73 pct of cold rolling, 700 μm × 700 μm EBSD scans were obtained with 1 μm step size.

Before EBSD, the samples were prepared with mechanical polishing down to 0.25 μm followed by electrochemical polishing with the STRUERS A2 electrolyte at 5 °C for 8 seconds and 26 V. After electrochemical polishing the samples were polished with STRUERS UP-U NonDry (Non-drying colloidal silica suspension with 40 nm particle size) for 8 hours. The scanning electron microscope (SEM) was operated at an acceleration voltage of 20 kV and a beam current of 12 nA.

The values of strain rate sensitivity to be used in crystal plasticity simulations were obtained from tensile tests performed at a temperature of 100 °C and at strain rates of 1, 10, 100, and 1000 s^{-1}. For rolling simulations, there is no preference for tension or compression to extract strain rate sensitivity values for cold rolling. Engler et al.[19] previously used tensile tests to obtain the strain rate sensitivity value of an alloy AA 6016 from room temperature up to 510 °C and for Al 8090 alloy from room temperature up to 450 °C.[12] Tensile tests guarantee a uniform stress state until necking while compression tests can lead to bulging and to a heterogeneous deformation state in the sample. Moreover, the strength differential effect or the tension-compression asymmetry are absent or limited in aluminum alloys. Holmen et al.[23] tested the alloys AA 6070 and AA 6060 in temper O (annealed) and in T6 and T7 states both in tension and compression at strain rates of 10^{-4} s^{-1} at room temperature. Temper O state exhibits no difference between axial stress in tension or compression. Only for T6 and T7 tempers the axial compression stress is 10 to 20 MPa higher than the tensile axial stress. Yan et al.[24] investigated the difference of strain rate sensitivity in tension and compression for a hot rolled 5A06 aluminium alloy (known as Russian standard AMΓ6 aluminium alloy and containing 6 wt pct of Mg and 0.6 wt pct of Mn) in state H112 at room temperature in the range of strain rates from 0.001 to 5000 s^{-1}, concluding that the m values under tension and compression are similar within the tested strain range of 0.05 to 0.25.

The temperature of 100 °C was chosen for the tensile tests because of the heating accumulated due to the speed of cold rolling in the industrial process. At least three tensile tests for each condition were performed.
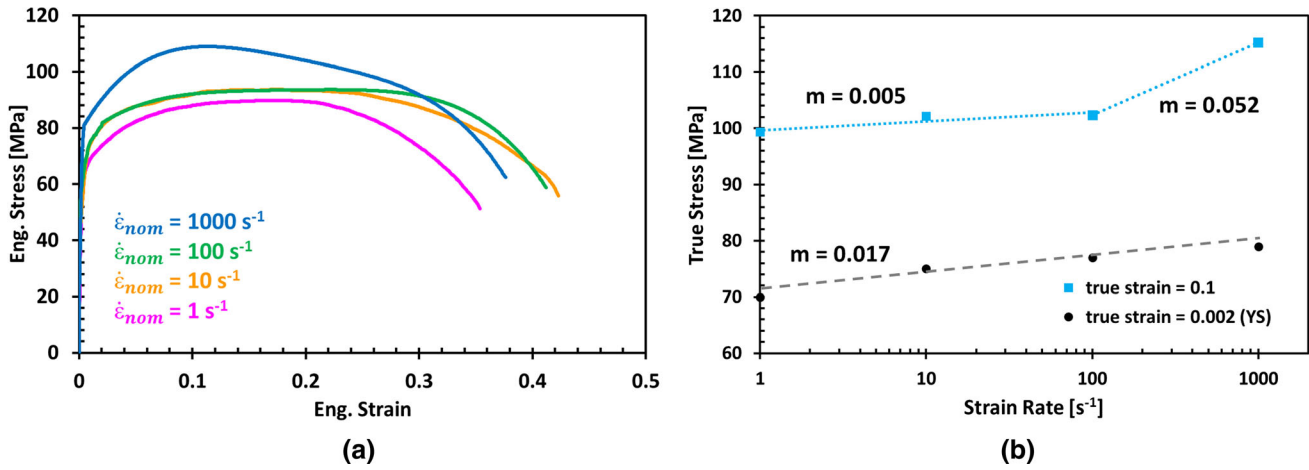
Fig. 3—One set of engineering stress–strain curves obtained on an Al6016 hot band at 100 °C and different strain rates (*a*) and values of flow stress at 0.002 (e.g. yield stress (YS)) and 0.1 of true plastic strain obtained experimentally as function of strain rate at a temperature of 100 °C (*b*).

Figure 3(a) shows one tensile curve for each strain rate, while Figure 3(b) shows the values of the yield stress and of the true flow stress at a plastic strain of 0.1 as function of strain rate. The values of strain rate sensitivity were calculated using the experimental flow stress values according to:

$$m = \frac{\log\left(\frac{\sigma_2}{\sigma_1}\right)}{\log\left(\frac{\dot{\varepsilon}_2}{\dot{\varepsilon}_1}\right)} \qquad [1]$$

where σ_1 is the true flow stress obtained at strain rate $\dot{\varepsilon}_1$ and σ_2 is the true flow stress obtained at strain rate $\dot{\varepsilon}_2$. The tensile tests were performed at the Fraunhofer Institute for Mechanics of Materials IWM—Crash Safety and Damage Mechanics department using a high speed testing machine type Instron VHS100-20 (maximum load 100 kN and maximum speed 20 m/s). Cylindrical tensile samples with a cross-section of 3 mm in diameter and a gauge length of 12 mm were extracted from the hot band. These sample size was selected according to the test standard used to extract material properties for crash simulations DIN EN ISO 26203-2[25] and FAT-guidelines.[26]

From these experiments, two values of strain rate sensitivity were calculated, one in the range of strain rate from 1 to 100 s^{-1} and another one in the range from 100 to 1000 s^{-1}. The values found were 0.005 and 0.052, respectively, for the true plastic strain of 0.1. These values were compared with values in literature. Recently, a value of 0.007 for tensile tests in the strain rates range from 0.1 to 100 s^{-1} was found for Al6016-T6,[27] while a value of 0.0377 was found for Split Hopkinson Tensile Bar (SHTB) tests in the range of strain rates from 380 to 1750 s^{-1}.[18] The obtained values of 0.005 and 0.052 are used in crystal plasticity simulations. Further higher strain rate sensitivity values (*i.e.* 0.071, 0.1 and 0.2) are used for the simulation of cold rolling to further assess the dependence of texture evolution on small variations of strain rate sensitivity because during a rolling step the local strain rate is not

constant during the deformation and variations of *m* can occur.

III. COLD ROLLING CRYSTAL PLASTICITY SIMULATIONS

Two aluminium Al6016 microstructures obtained from electron back-scattered diffraction (EBSD) scans performed at the center of an RD-ND section of the initial hot band were used to generate representative volume elements (RVEs) for crystal plasticity simulations with the freeware software package DAMASK.[28]

Two RVEs were obtained, the first one considering a smaller EBSD area of 400 μm × 400 μm containing a high percentage of Cube-oriented grains and with high resolution to track in detail the morphology evolution of Cube grains as function of strain rate sensitivity. A second RVE was constructed taking a larger EBSD area of 2850 μm × 2260 μm with smaller resolution but a larger amount of orientations (grains) pertaining to Cube and Brass to compare the final texture with the results obtained from the 400 μm × 400 μm RVE and with the experimental results.

DAMASK input files were created by writing a pipeline in DREAM.3D[29] to import microstructures cropped from EBSD scans. The two RVEs were then deformed in plane strain compression applying the compression history for the deformation gradient component along ND (F$_{33}$) as given in Table II, while the component F$_{22}$ was set to 1.0. The shear components F$_{12}$, F$_{13}$, F$_{23}$ of the deformation gradient were all set to zero.

In finite strain crystal plasticity (CP), the kinematics is described by the multiplicative decomposition of deformation gradient as:

$$\boldsymbol{F} = \boldsymbol{F}_e \boldsymbol{F}_p \qquad [2]$$

where $\boldsymbol{F}_e$ accounts for rigid body rotations and elastic distortion of the lattice, while $\boldsymbol{F}_p$ represents the plastic

part of deformation gradient and for the evolution of plastic deformation, only this part of the deformation gradient is of interest. $\boldsymbol{F}_\mathrm{p}$ contains the plastic shear deformation due to slip in crystalline planes and directions. The plastic deformation gradient evolves as

$$\dot{\boldsymbol{F}}_\mathrm{p} = \boldsymbol{L}_\mathrm{p}\boldsymbol{F}_\mathrm{p} \qquad [3]$$

where $\boldsymbol{L}_\mathrm{p}$ is the plastic velocity gradient formulated as sum of the shear rates on all slip systems according to:

$$\boldsymbol{L}_\mathrm{p} = \dot{\boldsymbol{F}}_\mathrm{p}\boldsymbol{F}_\mathrm{p}^{-1} = \sum_{\alpha=1}^{n} \dot{\gamma}^\alpha \boldsymbol{m}^\alpha \otimes \boldsymbol{n}^\alpha \qquad [4]$$

where $\boldsymbol{m}^\alpha$ is a vector representing the slip direction and $\boldsymbol{n}^\alpha$ is the vector of the normal to the slip plane of slip system α, while $\dot{\gamma}^\alpha$ is the shear rate of the αth slip system and n is the number of slip systems. In cold rolling simulations, only the twelve octahedral slip systems (i.e. $\{111\}\ \langle110\rangle$) are considered in the calculation of the plastic velocity gradient, while for hot rolling the twelve octahedral slip systems plus the six non-octahedral slip systems (i.e. $\{110\}\ \langle110\rangle$) are taken into account.

The constitutive behavior of aluminium was described using a phenopower law as implemented in DAMASK,[28] whose parameters are listed in Table III for cold rolling.[30] In phenomenological constitutive models,[31] the shear rate on slip system α is a function of a critical resolved shear stress (τ_c^α) and the resolved shear stress for slip system α (τ^α) according to:

$$\dot{\gamma}^\alpha = \dot{\gamma}_0 \left| \frac{\tau^\alpha}{\tau_c^\alpha} \right|^{1/m} \mathrm{sign}(\tau^\alpha) \qquad [5]$$

where $\dot{\gamma}_0$ is the reference shear strain rate and m is the strain rate sensitivity exponent. The evolution of the critical resolved shear stress is expressed as:

$$\dot{\tau}_c^\alpha = \sum_{\beta=1}^{n} h_{\alpha\beta} \left| \dot{\gamma}^\beta \right| \qquad [6]$$

This equation describes the influence of any set of slip system (index β) on the hardening behavior of a (specific) slip system α through the hardening matrix ($h_{\alpha\beta}$). This hardening matrix that captures the micromechanical interaction among different slip systems is given by:

$$h_{\alpha\beta} = q_{\alpha\beta} \left[h_0 \left(1 - \frac{\tau_C^\beta}{\tau_s} \right)^a \right] \qquad [7]$$

with h_0, a and τ_s representing the self-hardening coefficient, the hardening exponent, and the saturation value of slip resistance respectively. These parameters are assumed to be identical for all FCC slip systems. The parameter $q_{\alpha\beta}$ is calculated as:

$$q_{\alpha\beta} = (q_{lat} + (q_{self} - q_{lat})\delta_{\alpha\beta}) \qquad [8]$$

where $\delta_{\alpha\beta}$ is the Kronecker delta and q_{self} and q_{lat} are the self and latent hardening respectively. The hardening matrix contains diagonal terms (q_{self}) and off-diagonal terms (q_{lat}). The latent hardening is set to 1.0 for coplanar slip systems and 1.4 for non-coplanar slip systems to make the hardening model anisotropic. These values were found to agree with experimental studies and they were previously used for texture analyses of FCC polycrystals.[13,32,33]

During deformation of a polycrystalline RVE, the initial grid of material points is distorted because of deformation heterogeneity in each grain. When this distortion becomes too large, the mechanical problem associated to stress equilibrium cannot be solved and convergence is not reached. To simulate thickness reduction higher than 40 to 50 pct or deformations with very low values of strain rate sensitivity, where convergence becomes difficult because of plastic strain localization, a remeshing scheme was recently implemented in DAMASK. During the remeshing, a new undistorted grid is created and the state variables from the previous deformation step are mapped into the newly created grid using a nearest-neighbor mapping algorithm. The next cold rolling step can then be performed with the new undistorted grid. During remeshing, the elastic deformation is relaxed. A detailed description of the implemented remeshing scheme is described in Sedighiani et al.[34]. A remeshing step was performed at the end of each rolling step indicated in Table II before starting the next compression step.

As already mentioned, depending on alloy composition and microstructure, aluminium alloys exhibit a wide range of values for the strain rate sensitivity exponent (m).

If the aluminium alloy has a high strain rate sensitivity exponent, the rolling speed is expected to affect texture development. A series of crystal plasticity simulations were performed by modifying the m value and the evolution of texture components was assessed by calculating the volume fraction of standard rolling components (Cube, ND rotated Cube, Brass, Goss, Copper and S orientations) and other components (invGoss, P and Q orientations), considering a maximum misorientation of 15 deg. The crystallographic orientations of the calculated texture components are listed in Table IV. The values of m that were simulated are:

- m of 0.005 (i.e. $1/m$ equal to 200 in the phenopower law) (to be compared with rolling experiments);
- m of 0.0522 (i.e. $1/m$ equal to 19 in the phenopower law) (to be compared with rolling experiments);
- m of 0.071 (i.e. $1/m$ equal to 14 in the phenopower law);
- m of 0.1 (i.e. $1/m$ equal to 10 in the phenopower law);
- m of 0.2 (i.e. $1/m$ equal to 5 in the phenopower law);

The volume fraction of the rolling texture components was plotted as function of thickness reduction for different strain rate sensitivity values. The fraction for the rotated Cube is not included in the plots because at the end of the rolling process its fraction was always below 0.1 pct for all experiments and simulations.

Table II. Number of Rolling Passes Simulated in DAMASK for Cold Rolling of Al6016 With the F_{33} Value Implemented in the Simulation and the Corresponding Thickness Reduction

Rolling Pass	F_{33}	Thickness Reduction Per Pass (Pct)	Total Thickness Reduction (Pct)
1st	0.75	25	25
2nd	0.86	14	35.5
3rd	0.93	7	40
4th	0.91	9	45.4
5th	0.92	8	49.8
6th	0.93	7	53.3
7th	0.94	6	56
8th	0.94	6	58.7
9th	0.94	6	61.2
10th	0.94	6	63.5
11th	0.90	10	67.2
12th	0.93	7	69.5
13th	0.92	8	72

Table III. Parameters of the Phenopower Law Used in DAMASK for Cold Rolling Simulations

Parameter	Value
C_{11}	106.75 GPa
C_{12}	60.41 GPa
C_{44}	28.34 GPa
$\dot{\gamma}_0$	0.001 s^{-1}
$1/m$	see text
τ_c^β	31 MPa
τ_s	63 MPa
a	2.25
h_0	75 MPa
$q_{\alpha\beta}$ (Self and Coplanar Slip Systems)	1.0
$q_{\alpha\beta}$ (Non-coplanar Slip Systems)	1.4

Table IV. Crystallographic Orientations Analyzed During Evolution of Texture for Aluminium Microstructures

Crystallographic Orientation	$\{hkl\}$ || ND + $\langle uvw \rangle$ || RD
Cube	$\{001\}$ $\langle 100 \rangle$
ND Rotated Cube	$\{001\}$ $\langle 110 \rangle$
Brass	$\{110\}$ $\langle 112 \rangle$
S	$\{123\}$ $\langle 634 \rangle$
Copper	$\{112\}$ $\langle 111 \rangle$
Goss	$\{011\}$ $\langle 100 \rangle$
Q	$\{013\}$ $\langle 2\text{-}31 \rangle$
P	$\{011\}$ $\langle 122 \rangle$
invGoss	$\{0\text{-}11\}$ $\langle 011 \rangle$

IV. RESULTS AND DISCUSSION

A. Texture Volume Fractions and Cube Morphology Obtained in Cold Rolling Experiments

Figure 4 shows the IPF for normal direction (ND) of the RD-ND sections of the two 55 pct cold rolled microstructures. The distribution of grains pertaining to Cube orientations is shown for each microstructure considering their misorientation and the (111) pole figures are included. Both cold rolled microstructures have developed the β fiber components (Copper, S and Brass). However, the sample rolled at a speed of 600 m/min shows a higher maximum intensity for the ODF plot in the (111) pole figure and a higher intensity close to Cube orientation than the microstructure for rolling at 80 m/min. Cube grains appear elongated in both rolled microstructures but Cube fragmentation is higher for rolling at 80 m/min. Figure 5 shows experimental RD-ND sections with [001] inverse pole figures colors, Cube distribution maps and (111) pole figures after 72 to 73 pct thickness reduction for both speeds. At this thickness reduction, the two microstructures do not show significant differences in terms of Cube intensity.

To quantify these results, the volume fraction of several texture components is plotted for all samples in Figure 6(a), while Figure 6(b) shows the volume fraction of Cube texture depending on its misorientation angle from the exact Cube orientation.

In Figure 6(a), both cold rolled microstructures have lower Cube volume fraction than the initial hot band, with an increase of Brass, Copper and S (*i.e.* beta fiber) components. At 55 pct thickness reduction, the final Cube volume fraction is 4 pct higher in the sample rolled at 600 m/min. In this sample, the volume fraction of Copper is 5 pct higher than for rolling at 80 m/min. At 55 pct reduction, Brass and Goss orientations are not affected significantly from changes in rolling speed (*i.e.* the difference between the rolled samples is within 1 pct, with Brass higher for 600 m/min and Goss higher for 80 m/min). The volume fraction of S is 3 pct higher for 80 m/min. Inverse Goss, Q and P orientations are not affected by different rolling speeds. At 73 pct thickness reduction, the amount of Cube decreases to 2.7 pct for both speeds. The Brass fraction is not affected, while Copper is 5 pct higher for the lamination speed of 600 m/min and the S texture increases in both samples but the difference of volume fraction between the two speeds is only 2 pct. Inverse Goss, Q and P are not affected by changes in
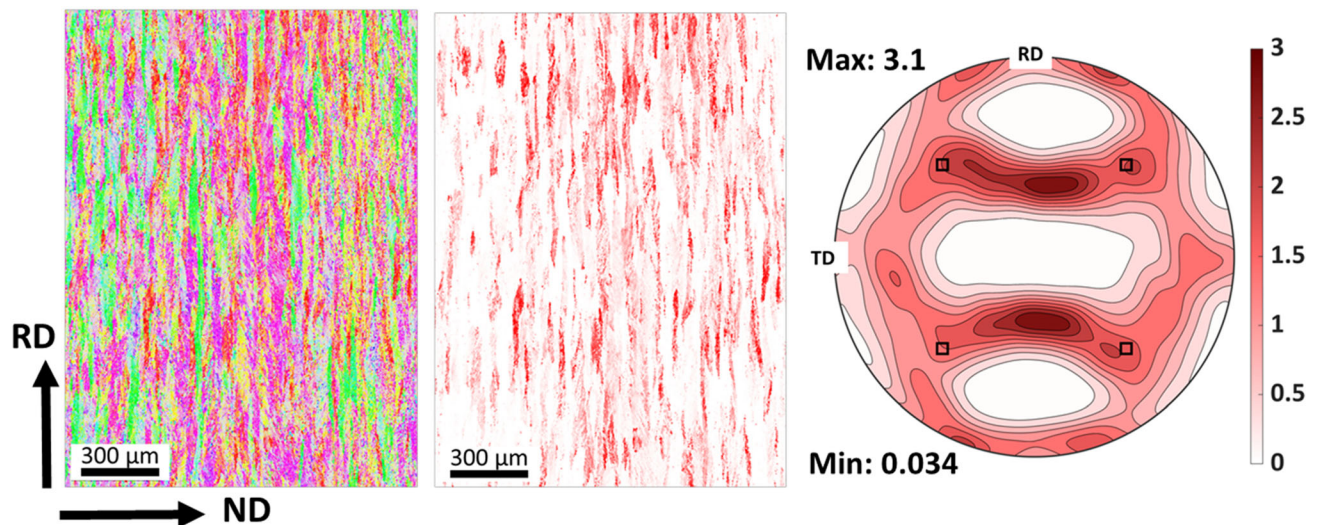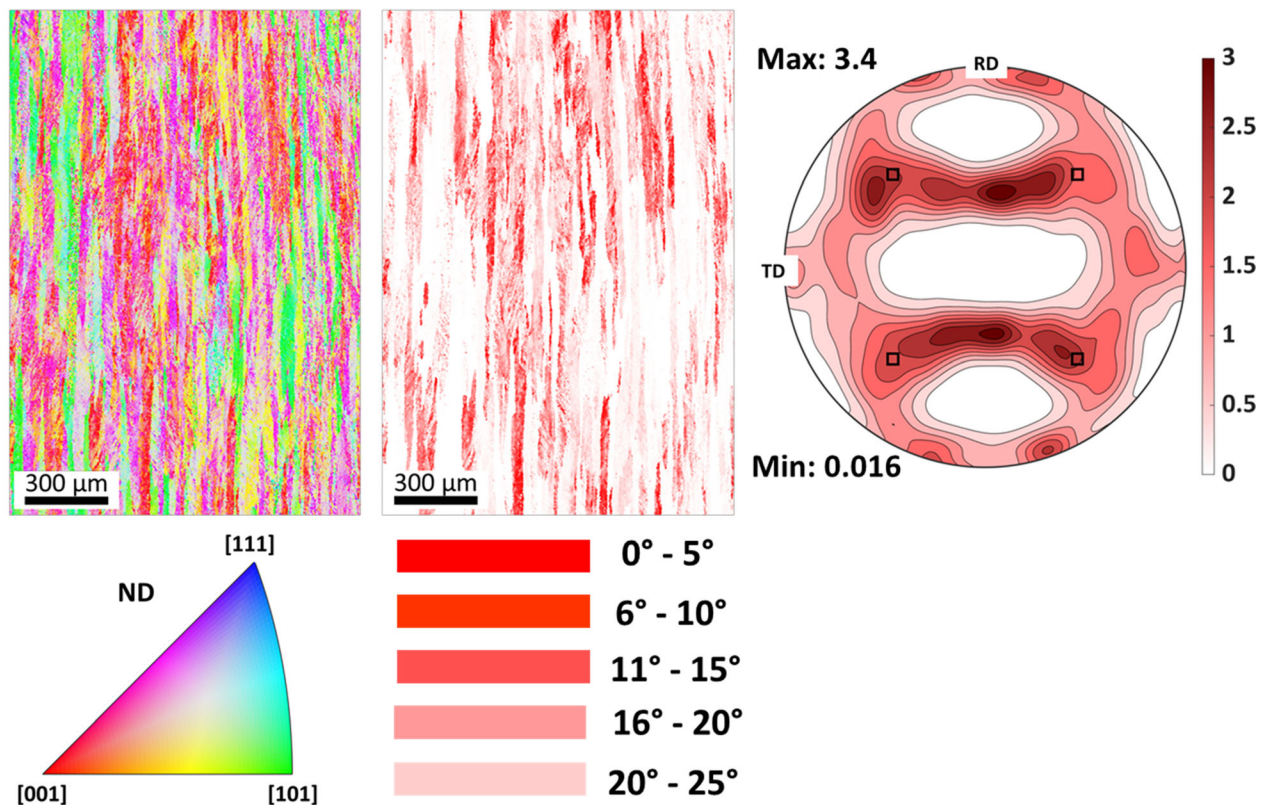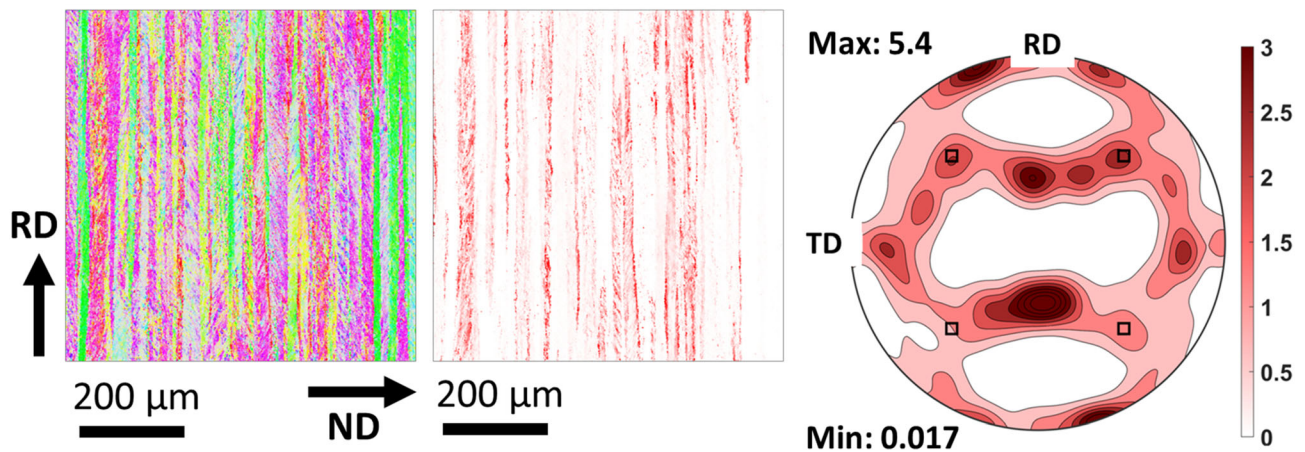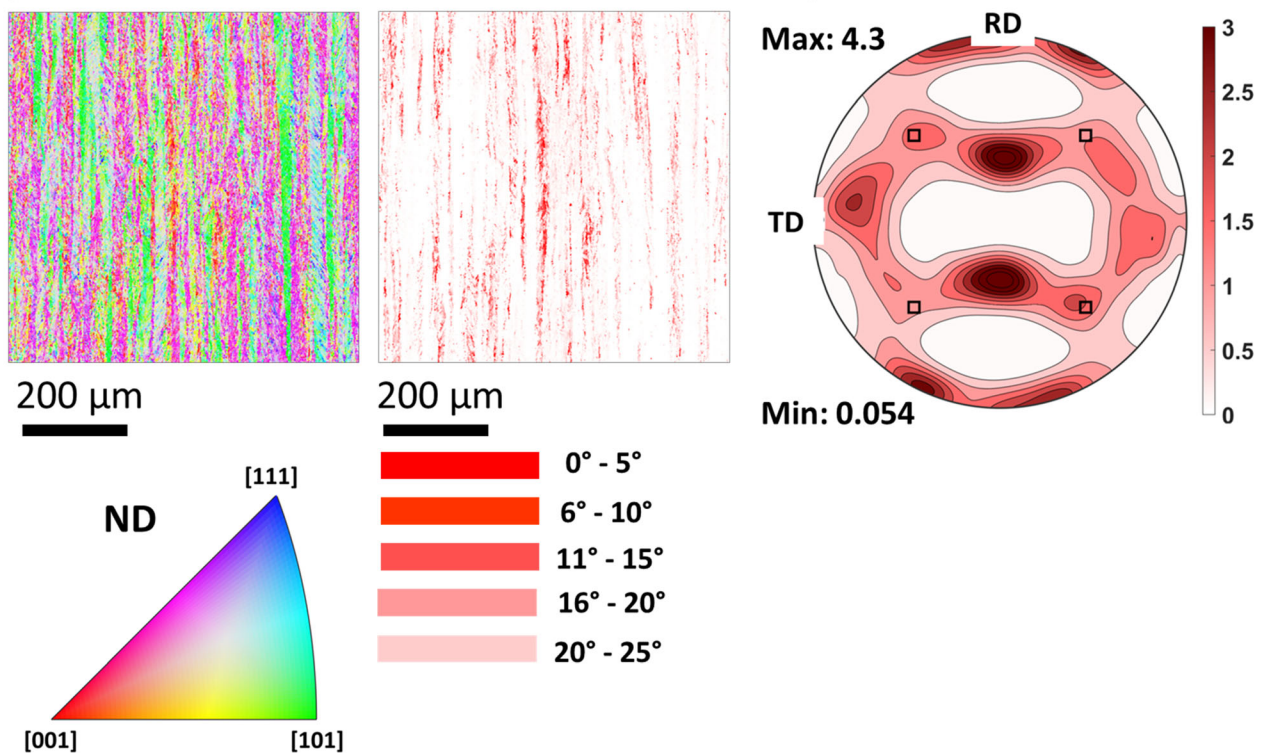
Fig. 4—IPF for normal direction (ND) (images on the left) for microstructures after 55 pct cold rolling at 80 m/min and 600 m/min. At the center, distribution of grains having Cube orientation (with max. 25 deg misorientation) and on the right (111) pole figures of the whole microstructure.

rolling speed even at 73 pct thickness reduction. In Figure 6(b), for 55 pct thickness reduction, the Cube volume fractions with 6 to 10 deg or 11 to 15 deg misorientation are higher for cold rolling at 600 m/min confirming that Cube fragmentation is delayed or hindered more than rolling at 80 m/min. Interestingly the difference among the two speeds is negligible for

Cube misoriented between 0 and 5 deg. With further thickness reduction, the difference between the two speeds is further reduced and the 2.7 pct of total Cube remaining in the microstructure shows 6 to 15 deg misorientations. These experimental results indicate that Copper and Cube are the orientations more affected by changes of strain rate sensitivity.

Microstructure after cold rolling at 80 m/min (73% CR)

Microstructure after cold rolling at 600 m/min (73% CR)

Fig. 5—IPF for normal direction (ND) (images on the left) for microstructures after 73 pct cold rolling (CR) at 80 m/min and 600 m/min. At the center, distribution of grain having Cube orientation (with max. 25 deg misorientation) and on the right (111) pole figures of the RD-ND sections.

B. Cold-Rolling Crystal Plasticity Simulations

Figure 7 shows the texture evolution for the most important crystallographic orientations as function of thickness reduction for different values of strain rate sensitivity. Simulations were performed up to a compression of 73 pct (*i.e.* final thickness of 1.08 mm) to show that for strain rate sensitivity values equal or higher than 10^{-2}, Cube fragmentation is delayed and a higher compression is required to decrease its volume fraction. However, for comparison with industrial rolling specimens, the texture at 55 pct compression was extracted from simulations (the dashed gray line in Figure 7 is drawn at 55 pct thickness reduction). From Figure 7(a), at 55 pct thickness reduction, the remaining Cube volume fraction is 0.9 pct for an *m* of 0.005 and 3.3 pct for 0.052. With a further increase in strain rate sensitivity to 0.071, 0.1 and 0.2, the Cube fraction rises to 4.5, 6.1 and 12.4 pct respectively. The Brass amount at 55 pct thickness compression is 7.1 pct for *m* equal to 0.005 and 7.9 pct if *m* is 0.052 (Figure 7(b)). Brass texture increases with an increase of strain rate sensitivity, particularly if the thickness reduction is above 60
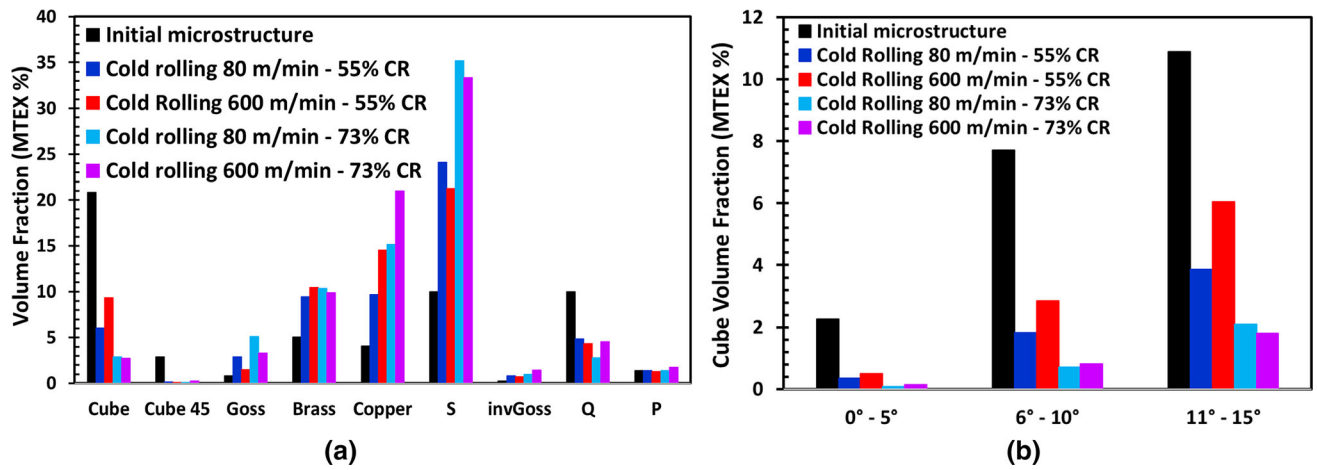
Fig. 6—Comparison of volume fractions of texture components for the starting hot band and for the cold rolled (CR) coils laminated at 80 m/min and 600 m/min (*a*). Comparison of Cube fraction as function of its misorientation from the exact Cube orientation for initial hot bands and the two cold rolled (CR) coils (*b*).

pct. Copper in Figure 7(c) increases when the strain rate sensitivity goes from 10^{-3} to 10^{-2}, but it does not vary if *m* is increased further to 0.1 or 0.2. For an *m* of 0.005, the Copper fraction is 4.2 pct and it reaches 6 pct for an *m* of 0.052. These simulation results confirm the tendencies of volume fractions that were found experimentally for Cube, Copper and Brass at 55 pct cold rolling reduction (Figure 6(a)).

The S texture component in Figure 7(d) has a value of 8.9 and 10.4 pct for an *m* of 0.005 and 0.052 respectively. Further increase of *m* to 0.1 or 0.2 gives the same volume fraction as found at 0.052. In experiments, the S volume fraction difference was at maximum 2 pct higher at 80 m/min than 600 m/min. The value of Goss (Figure 7(e)) is 1.7 pct both for *m* 0.005 and 0.052. Only if *m* is equal to 0.2 and thickness reduction is above 60 pct, then the strain rate sensitivity influences Goss.

As obtained in cold rolling experiments, Q, P and invGoss textures components are not affected significantly by variations of strain rate sensitivity. Only invGoss (Figure 7(h)) is higher for low values of *m* but its total fraction remains low in the microstructure.

In Figure 7, the initial microstructure contains a high Cube fraction and no other relevant texture component (except 6 pct of Q texture). For the first 20 to 25 pct of thickness reduction, the volume fraction of Cube diminishes rapidly promoting Brass formation (6 to 8 pct), while Copper and S amounts remain below 4 pct. For thickness reductions above 30 pct, the amount of Brass saturates and more Copper and S are formed. Microstructures containing strong Cube texture deformed at room temperature at different plastic strain confirmed this tendency for Cube to rotate towards Brass at low strains and to shift to beta fiber components (S and Copper) for higher compression strains.[14] With higher thickness reduction of 73 pct, the difference of Cube fraction between the two *m* values decreases (*i.e.* 0.22 pct for an *m* of 0.005 and 0.47 pct for an *m* of 0.052), but if strain rate sensitivity is 0.1 or 0.2, the Cube volume fraction left in the microstructure is 1.3 and 5 pct respectively. At 73 pct thickness reduction, Brass is 1

pct higher for the *m* of 0.052 than an *m* of 0.005, while experiments show 2 pct higher fraction for lower rolling speed. The difference in Brass fraction for these low *m* values is negligible, a higher Brass difference is expected to be found when *m* is above 10^{-2}. At 73 pct thickness reduction, the volume fraction of Copper is 3 to 4 pct higher for *m* equal or above 0.052 than the fraction found for an *m* of 0.005, as was obtained in experimental textures. At 73 pct reduction, a higher volume fraction of Goss is found for an *m* of 0.052 but in experiments a higher fraction was found for the lowest rolling speed.

Strain rate sensitivity has an influence on the morphology of the Cube texture left in the microstructure. The evolution of RD-ND microstructure for different values of *m* at 55 pct thickness reduction is shown in Figure 8. It was chosen to plot the IPF for the normal direction (ND) of the RD-ND sections at 55 pct cold rolling and not 73 pct because the grain fragmentation is not too strong and visual comparison is facilitated.

The same set of cold-rolling simulations was repeated on a larger area of 2850 μm × 2260 μm extracted from EBSD of the hot band to confirm these results. Contrary to the first RVE, this area contains an initial 25 pct of Cube orientation but significant amounts of Copper, S, Brass and Q texture are present. Figure 9 shows the volume fraction evolution of texture components as function of thickness reduction for different values of *m*. Stabilization of Cube for increasing values of m is confirmed (Figure 9(a)). In contrast to the first simulated microstructure, in this second set of simulations, the initial texture has 4 pct of Brass. This texture is stable for *m* values between 10^{-3} and 0.1 and it increases only when *m* is equal to 0.2 (Figure 9(b)). This low variation of Brass for *m* values in the range of 10^{-3} to 10^{-2} agrees with results shown in Figure 6(a). The previous trends of Copper, S and Goss evolution as function of strain rate sensitivity are confirmed also for this microstructure (Figures 9(c), (d) and (e)). Q, P and invGoss orientations are not affected by variations of strain rate sensitivity (Figures 9(f), (g) and (h)). For this RVE with an initial texture made of several
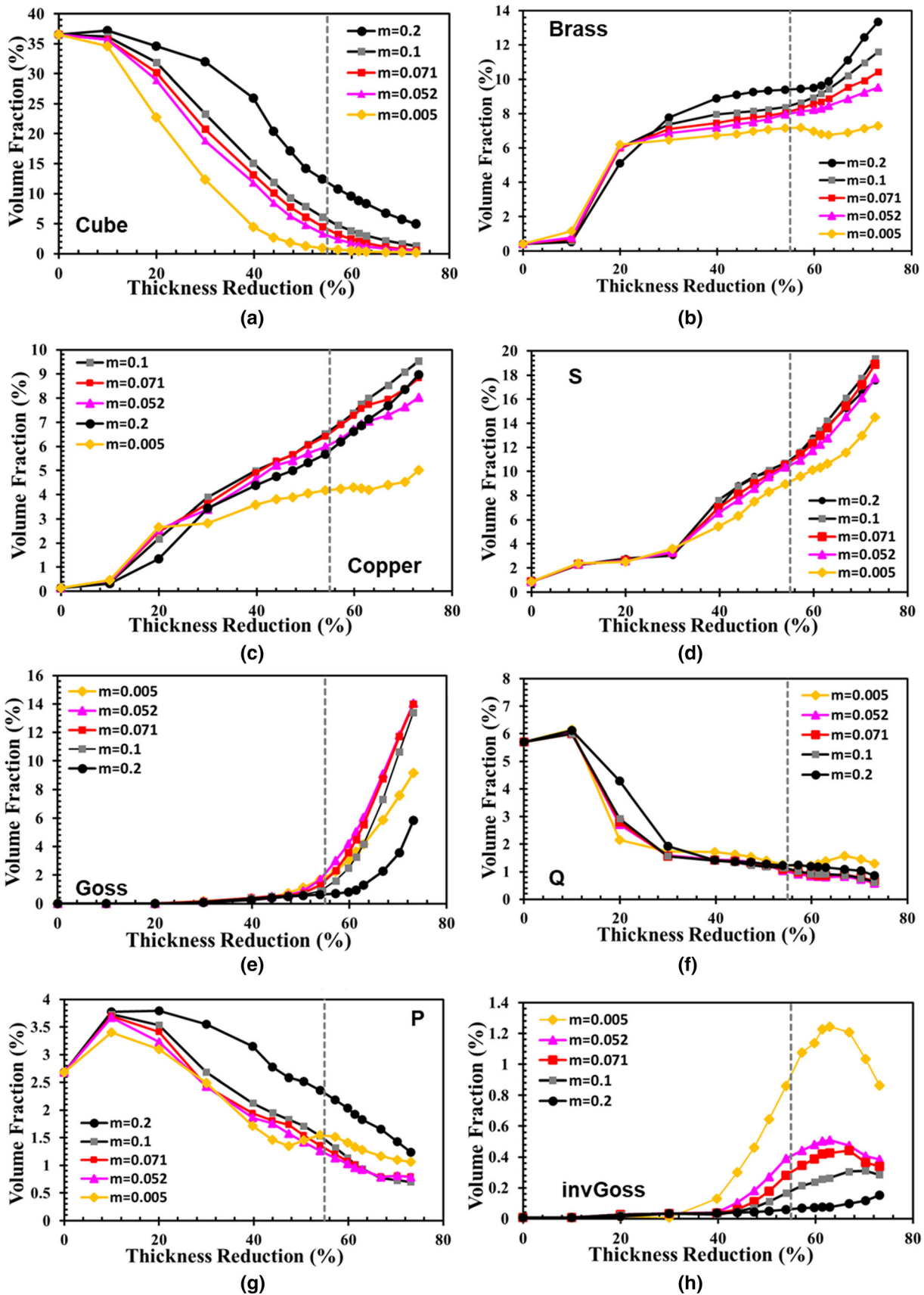
Fig. 7—Volume fractions as function of thickness reduction and strain rate sensitivity for several texture components ((a) through (h)) during cold rolling. Evolution extracted from crystal plasticity simulations performed on initial EBSD area of 400 μm $\times$ 400 μm.
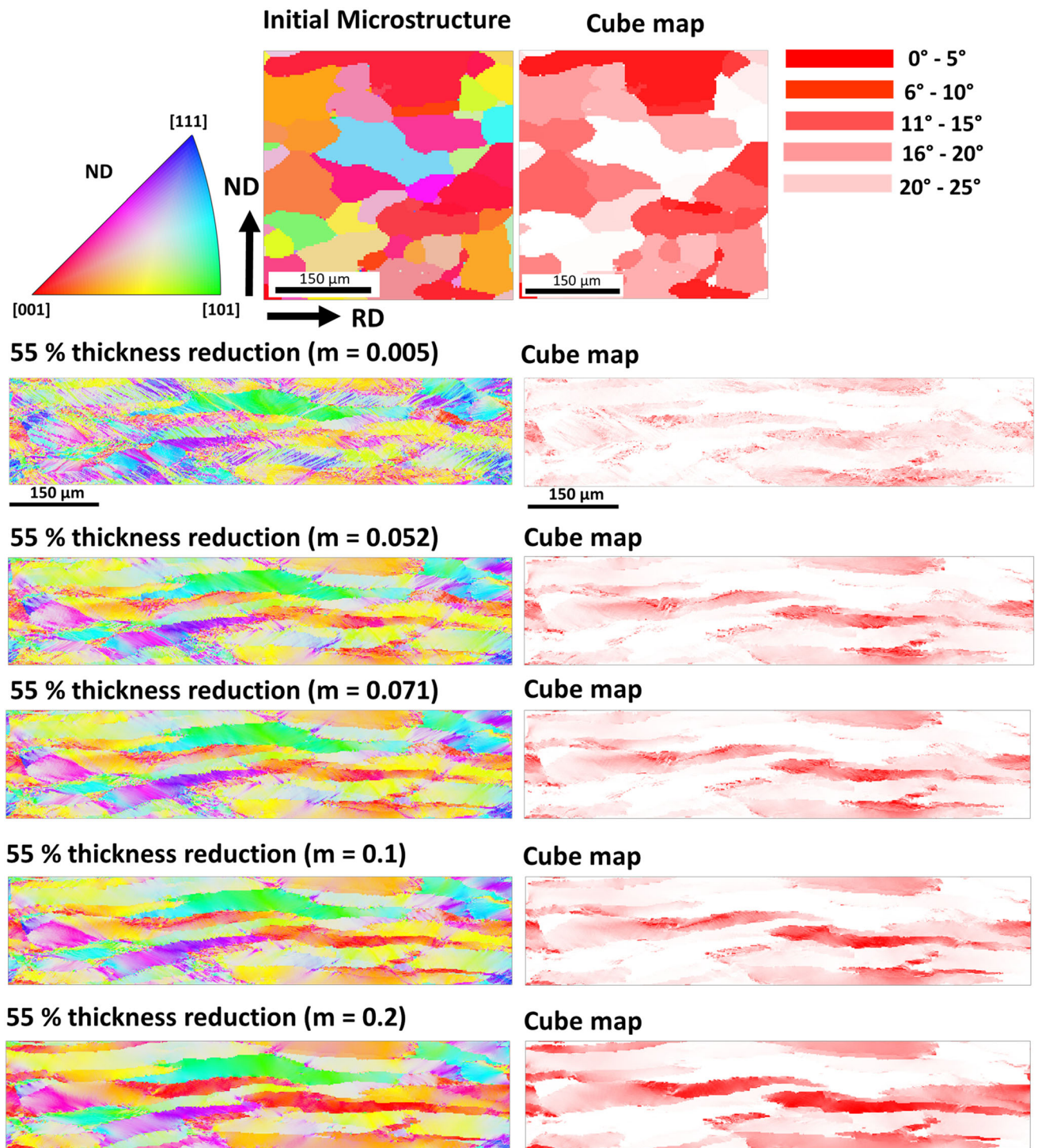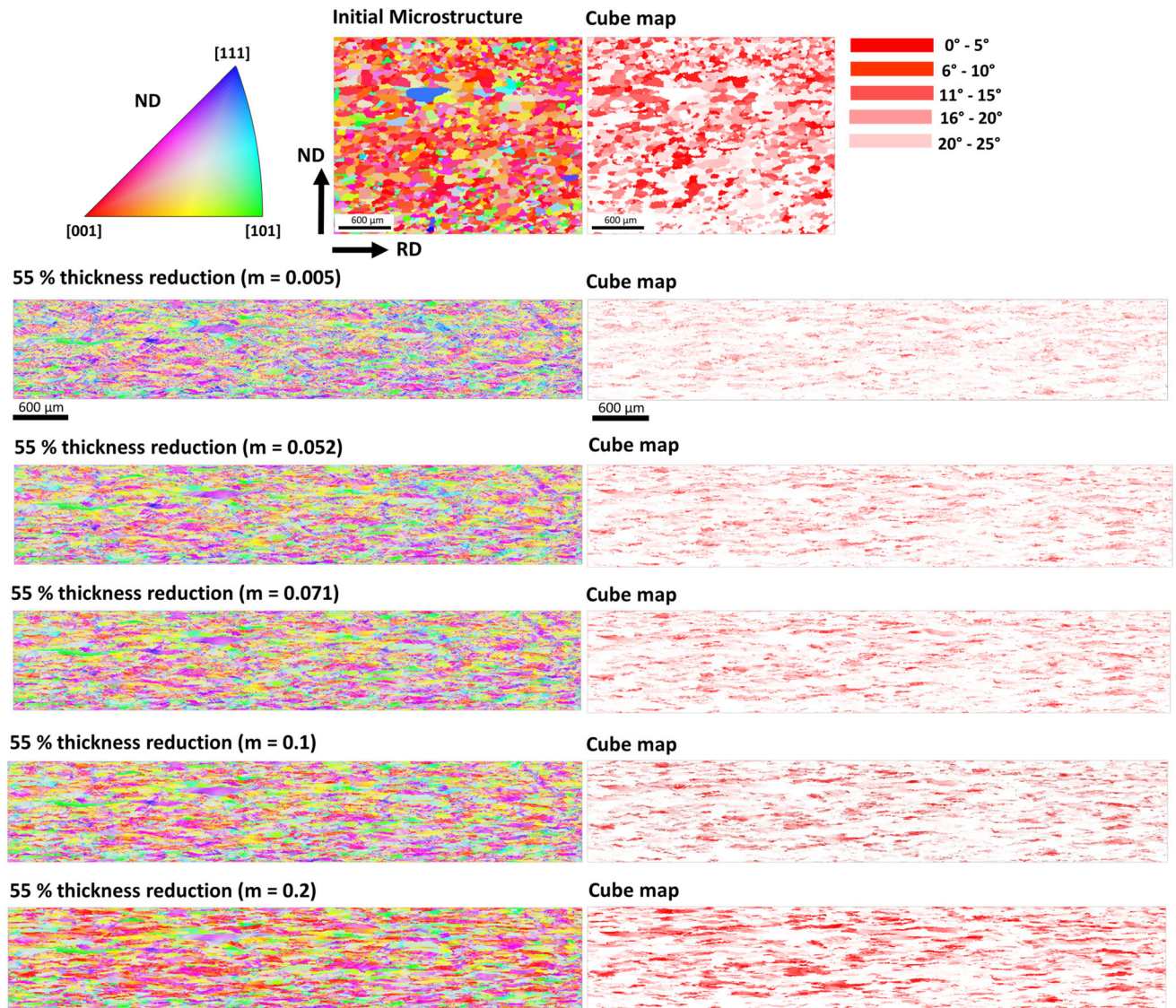
Fig. 8—Evolution of microstructure from crystal plasticity simulations in the RD-ND section for an initial Al 6016 microstructure (area 400 μm × 400 μm) for different values of strain rate sensitivity. Images on the left show the IPF for normal direction (ND) of the microstructure, while images on the right show distribution of grains pertaining to Cube orientation considering a maximum misorientation of 25 deg. Microstructures correspond to 55 pct thickness reduction.

components, for low thickness reductions (*i.e.* 20 to 25 pct) Cube decreases, but on the contrary from the first presented RVE, here formation of Copper and S is more favored than Brass. This confirms published experimental results where for both cold and hot rolling, initially random textures promote Copper formation at the expense of Brass. [14]

Figure 10 shows the RD-ND microstructures extracted from crystal plasticity simulations at 55 pct thickness reduction.
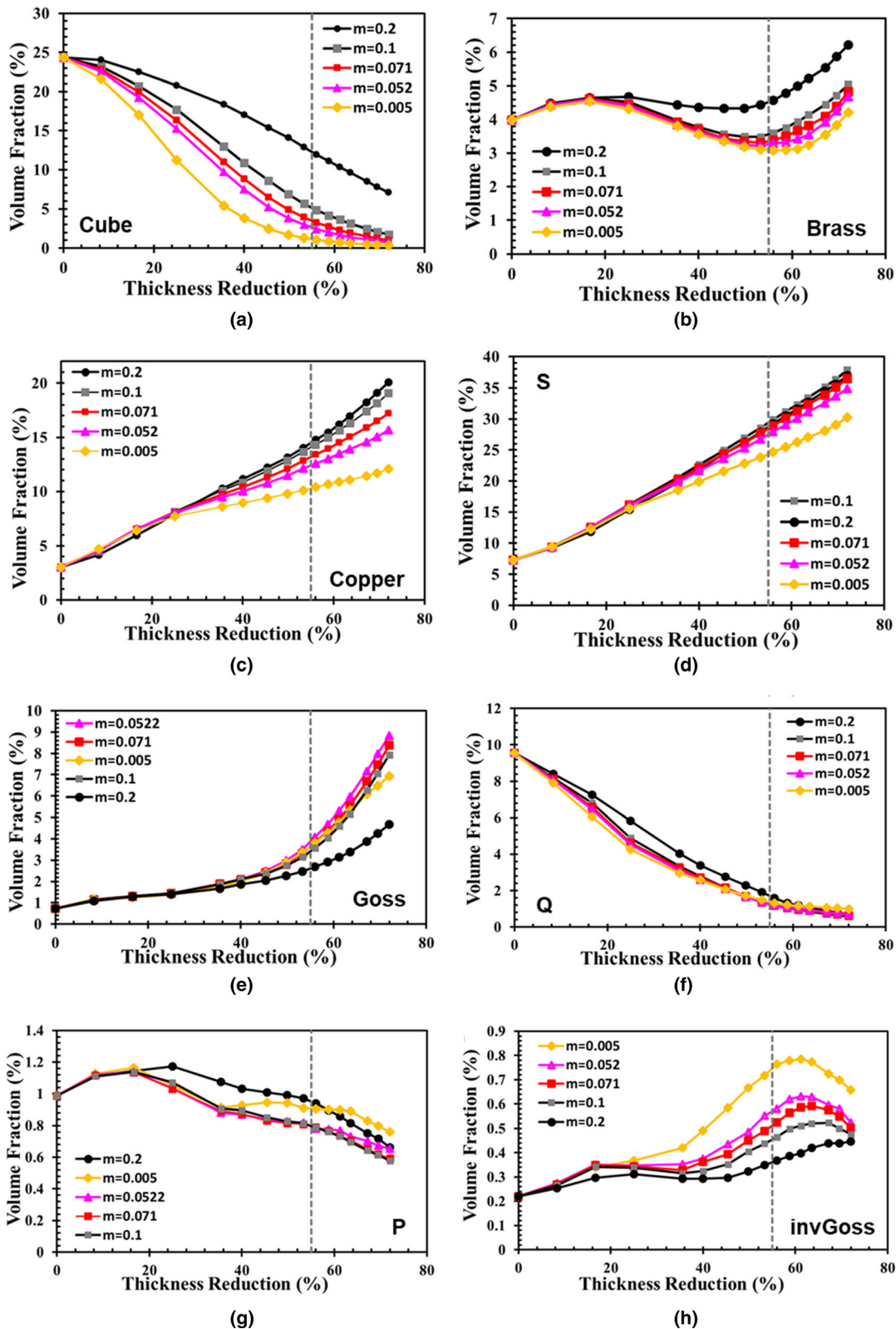
Fig. 9—Volume fractions as function of thickness reduction and strain rate sensitivity for several texture components ((a) through (h)) during cold rolling. Evolution extracted from crystal plasticity simulations performed on an intial EBSD area of size 2850 μm × 2260 μm.

Figures 11(a) and (b) show the distribution of Cube texture as function of degree of misorientation from exact Cube orientation for both initial microstructures (i.e. 400 μm × 400 μm and 2850 μm × 2260 μm) and 55 pct thickness reduction. Values of strain rate sensitivity in the order of 10^{-3} and 10^{-2} leave almost no Cube with

Fig. 10—Evolution of microstructure from crystal plasticity simulations in the RD-ND section for an initial Al 6016 microstructure (EBSD area of 2850 μm $\times$ 2260 μm) for different values of strain rate sensitivity. Images on the left show the IPF for normal direction (ND) of the microstructure, while images on the right show distribution of grains pertaining to Cube orientation considering a maximum misorientation of 25 deg. Microstructures correspond to 55 pct thickness reduction.

a misorientation below 5 deg but all the Cube remaining in the microstructure shows a misorientation between 6 and 15 deg with higher fraction of Cube for an m of 10^{-2} than 10^{-3}. An increase of strain rate sensitivity to 10^{-1} retains a 1.0 to 1.5 pct of Cube which is misoriented less than 5 deg in the microstructure. This suggests that high values of strain rate sensitivity favor Cube stabilization and can potentially form microstructures which are more prone to preferential growth of Cube grains during final recrystallization.

The trends of texture evolution as function of strain rate sensitivity from experiments were compared with the simulation results from the larger EBSD area (Figures 12(a) and (b) and 5). Brass, Goss, invGoss, Q and P do not show significant dependence on strain rate sensitivity both in experiments and simulations. Experimentally, at 73 pct thickness reduction, S has no

dependence on strain rate sensitivity but in simulations a 4 pct higher fraction is found for an m of 0.052. Cube and Copper are affected by strain rate sensitivity and the tendency is the same for both simulations and experiments. Looking at Figures 12(a) and (b), the total amount of Cube and Brass is underestimated in simulation compared to experiments. Table V summarizes the tendencies from experiments and simulations.

A comparison of ODF sections at 55 pct thickness reduction for the larger simulated microstructure (2850 μm $\times$ 2260 μm) for the two values of strain rate sensitivity of 0.005 (Figure 13) and 0.0522 (Figure 14) is done with ODF sections extracted from experiments. In Figure 13 and Figure 14, the intensity of the ODF is higher for the strain rate sensitivity of 0.052 than 0.005. The same conclusion is valid for the intensity of ODFs from experiments (Figure 13 and Figure 14). Thus,
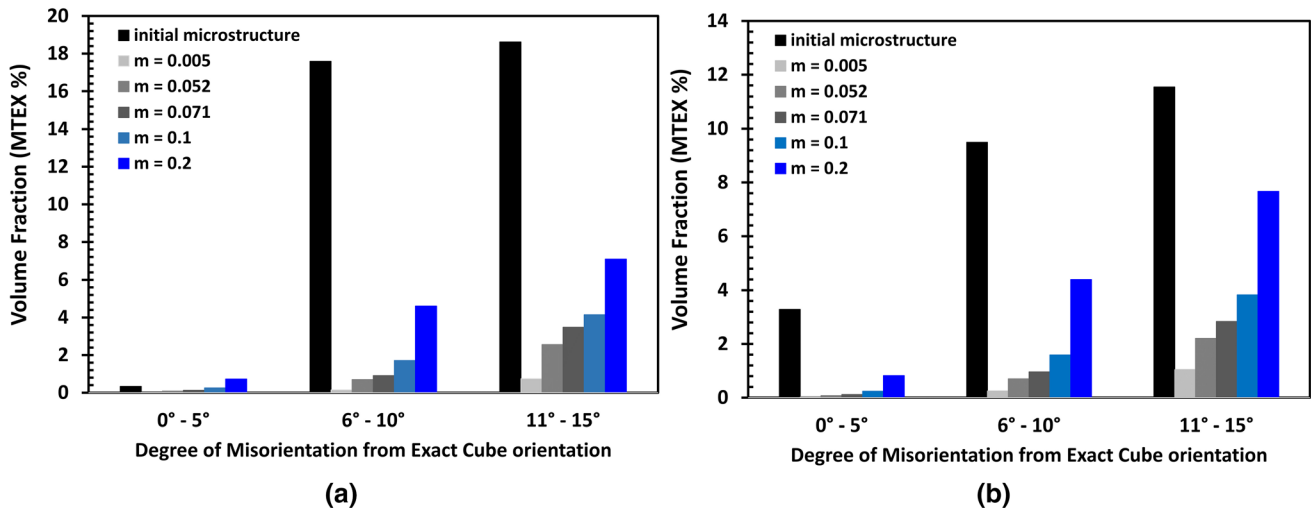
Fig. 11—Comparison of Cube fractions as function of its misorientation from the exact Cube orientation extracted from crystal plasticity cold rolling simulations for the initial microstructure of 400 μm $\times$ 400 μm (*a*) and for an initial microstructure of 2850 μm $\times$ 2260 μm (*b*) after 55 pct thickness reduction.
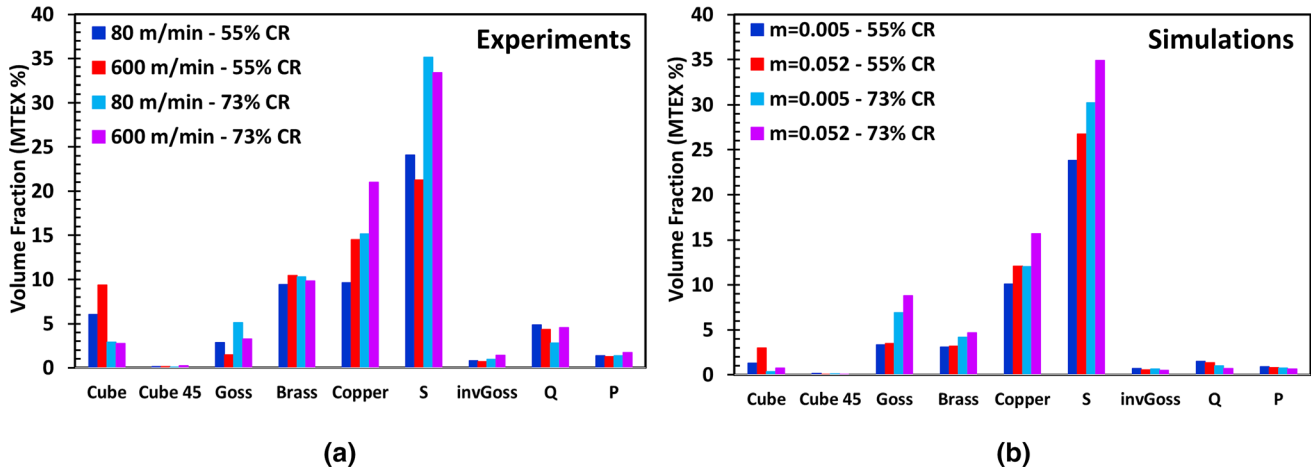

Fig. 12—Texture volume fraction from cold rolling (CR) experiments (*a*) and from crystal plasticity simulations with different strain rate sensitivities (*m*) (*b*).

Table V. Comparison Between Experiments and Simulations of Texture Evolution Tendencies as Function of Strain Rate Sensitivity

|	Experiments Comparison Between m of 0.005 and 0.052		Simulations Comparison Between m of 0.005 and 0.052	
Texture	55 Pct CR	73 Pct CR	55 Pct CR	73 Pct CR
Cube	$V_f \uparrow$ for $m\uparrow$	no difference	$V_f \uparrow$ for $m\uparrow$	no difference
Goss	1.4 pct higher V_f for $m\downarrow$	1.8 pct higher V_f for $m\downarrow$	no difference	1.8 pct higher V_f for $m\uparrow$
Brass	no difference	no difference	no difference	no difference
Copper	$V_f \uparrow$ for $m\uparrow$	$V_f \uparrow$ for $m\uparrow$	$V_f \uparrow$ for $m\uparrow$	$V_f \uparrow$ for $m\uparrow$
S	2.8 pct higher V_f for $m\downarrow$	1.7 pct higher V_f for $m\downarrow$	2.8 pct higher V_f for $m\uparrow$	4 pct higher V_f for $m\uparrow$
invGoss	no difference	no difference	no difference	no difference
Q	no difference	no difference	no difference	no difference
P	no difference	no difference	no difference	no difference
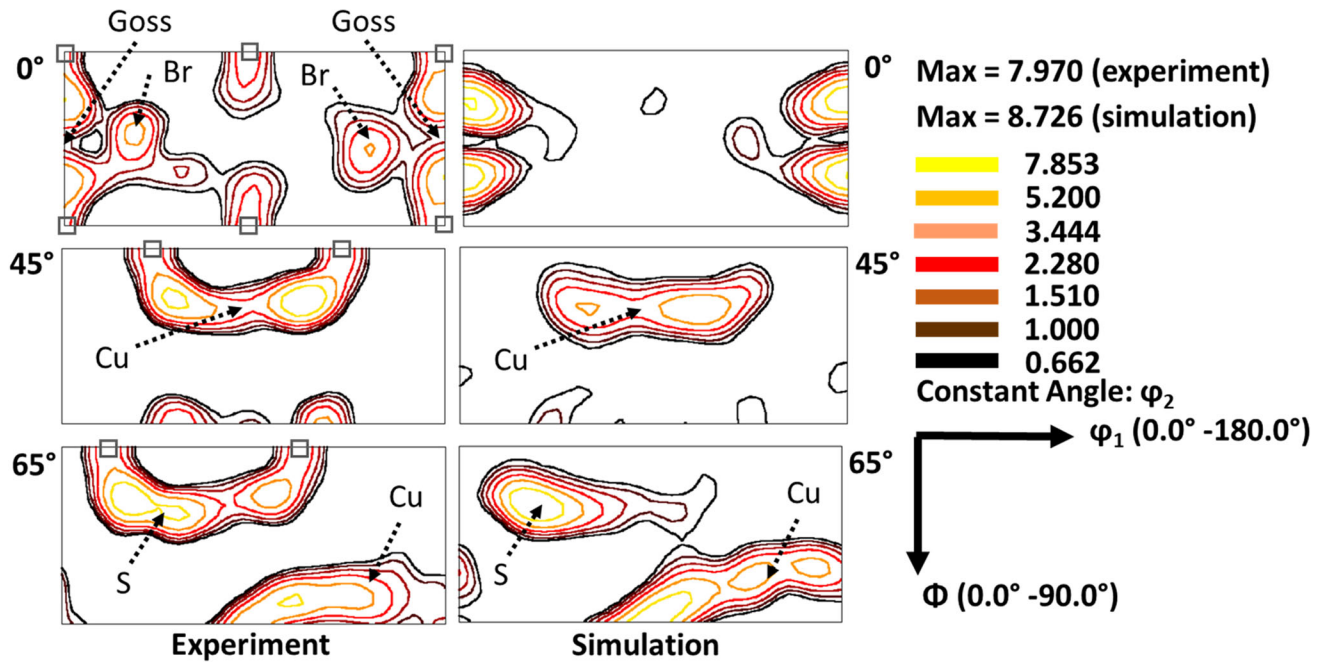
Fig. 13.—Comparison of ODF sections (0, 45, 65 deg) for microstructure cold rolled at 80 m/min (experiment) and DAMASK crystal plasticity simulation performed with a strain rate sensitivity of 0.005 (simulation) at 55 pct thickness reduction. Square markers indicate position of Cube texture, while position of Goss, Brass (Br), Copper (Cu) and S texture components is indicated by the black arrows.
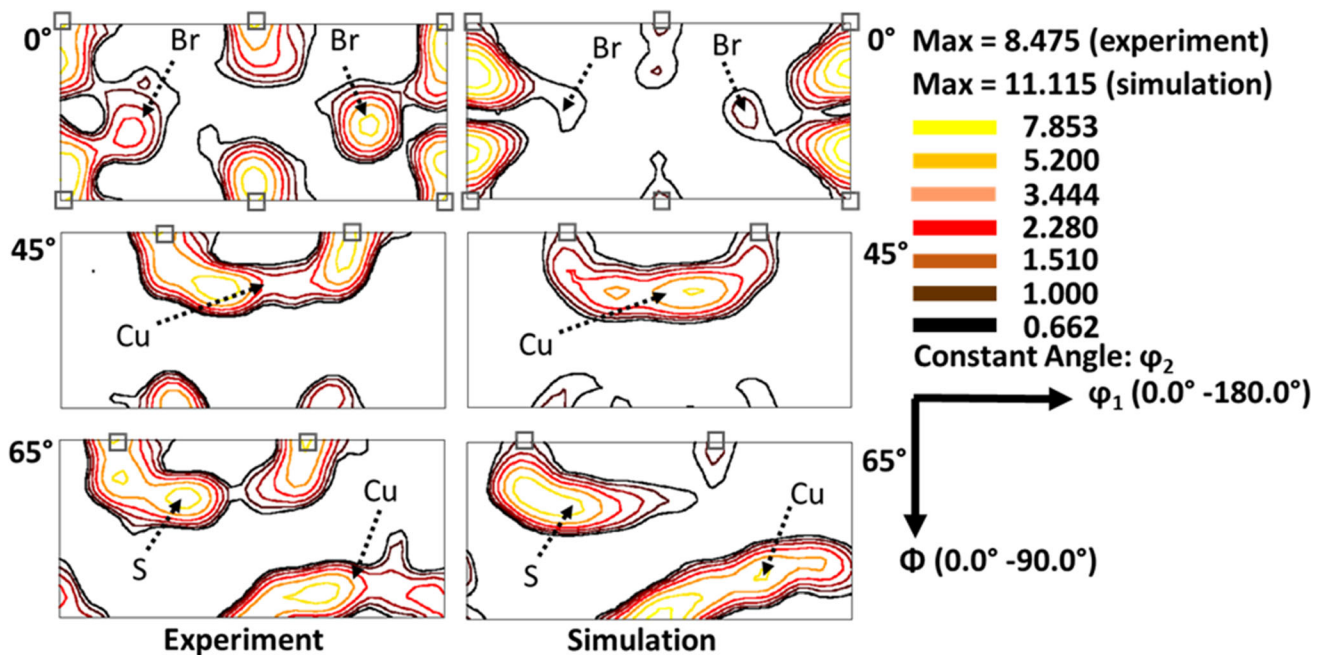

Fig. 14—Comparison of ODF sections (0, 45, 65 deg) for microstructure cold rolled at 600 m/min (experiment) and DAMASK crystal plasticity simulation performed with a strain rate sensitivity of 0.052 (simulation) at 55 pct thickness reduction. Square markers indicate position of Cube texture, while position of Brass (Br), Copper (Cu) and S texture components is indicated by the black arrows.

sharper texture is predicted for higher values of strain rate sensitivity. The texture components tendencies predicted through crystal plasticity simulations are consistent with the presented experimental results on aluminium. They differ from previous results of VPSC simulations, where Cube, Copper, S and Brass fractions were not well predicted for low values of strain rate sensitivity.[1] Moreover, VPSC calculation suggested that high values of m would cause a weaker texture intensity.[1] Canova et al.[35] and Asaro and Needleman[13] concluded that the intensity of texture is affected by loading; for uniaxial tension or compression in aluminium single crystals, high values of strain rate sensitivity increase the number of activated slip systems

and reduce the plastic spin causing a slower texture development. However, more recently, through compression tests on polycrystalline copper and nickel, Gurao et al.[36] have shown that the final intensity of texture as function of strain rate depends on strain hardening exponent. A high strain hardening exponent would prevent deformation heterogeneities thus preserving a strong texture.[36] The intensity of Cube texture is higher in the ODFs for specimens rolled at 600 m/min than specimens rolled at 80 m/min. Crystal plasticity simulations predict also higher Cube and texture intensity for a strain rate sensitivity of 0.052. However, experimentally more Cube texture is preserved in the microstructures for both rolling speeds than for crystal plasticity simulations, while the maximum intensity and the ODF shape of the beta fiber components is well predicted by crystal plasticity for both strain rate sensitivity values.

There can be several reasons for Cube volume fraction underestimation in simulations. First of all, in simulations, the texture evolution is always extracted from the same RD-ND zone, while experimentally the data are obtained from different RD-ND zones for several thickness reductions. This can be a limiting factor in predicting exact absolute values of volume fractions of texture components especially when the Cube distribution is not uniform through the thickness of the samples. Cube texture is known to be sensitive to small changes of loading and boundary conditions. In crystal plasticity, a perfect plane strain compression loading was simulated; however, during industrial cold rolling deviations from this loading condition are always present. In cold rolling, an RD axial tensile stress is present in the sheet because it is continuously pulled out of the hot rolled coil and the exact amount of this force cannot be estimated. Friction conditions can cause the rolling to be non-symmetric and evolution of friction values as function of time can affect the texture development. Moreover, modeling of friction and the associated shear loading can be difficult due to many parameters of the rolling plant influencing friction evolution.[37] Friction depends on rolling speed, temperature, composition of the rolling emulsion and surface finishing of the rolls. Furthermore, in crystal plasticity simulations (but more general in texture simulations), the m value in the phenopower law is considered equal to the macroscopic polycrystalline strain rate sensitivity, but the strain rate sensitivity of the slip systems could differ from the macroscopic m, as strain rate sensitivity could be also orientation dependent.[22] To exclude an influence from the simulation approach, further trials were performed on a hot band RVE containing a high Cube volume fraction and comparing results from 3D and 2D RVEs or reducing the number of remeshing steps, but these factors do not affect Cube volume fraction evolution (Figure A.1(a) in Appendix A and Figure B.1(a) in Appendix B). An improvement in Cube volume fraction prediction from crystal plasticity simulations was obtained by considering lower values for the latent hardening (i.e. 1.0 instead of 1.4). The only texture components affected by a change of this parameter are the Cube and Copper orientations (Figure C.1

in Appendix C)). Other lower values of hardening were investigated but they did not result in higher Cube volume fraction. Further simulations were performed changing the parameters a and h_0 in the phenopower law but always making sure to be close to the experimental tensile curve. However, the Cube volume fraction was changing less than 0.1 pct for a and h_0 variations.

The influence of latent hardening on rate-dependent texture evolution in finite strain Taylor models in polycrystals was discussed also by Asaro and Needleman,[13] concluding that isotropic or anisotropic hardening can affect texture evolution and that latent hardening is strain path dependent. This affects the history of activated slip systems resulting in different lattice rotations.

The underestimation of Brass is due to the use of a 2D RVE instead of a 3D RVE. As discussed in literature,[12,19] Brass texture is influenced by the presence or absence of ε_{12} strain and different amount of Brass were predicted if this strain component was fixed or relaxed. In the crystal plasticity rolling simulations, F_{12} was set to zero and in 2D RVEs where the is no grain boundary along the TD direction, this component of the deformation gradient is indeed zero. For 3D RVEs, however, where 3D grain boundaries are present, the F_{12} component is macroscopically zero, but locally can be non-zero. Thus, 2D RVEs can underestimate Brass while 3D RVEs allows better prediction of the total amount of Brass (as shown in Figures A.1(c) and (d)).

Despite the underestimation of the absolute value of Cube and Brass fractions, cold rolling crystal plasticity simulations capture well the influence of small changes in strain rate sensitivity on texture evolution. For this reason, the analysis was extended to hot rolling simulations for an initial microstructure containing a high fraction of Cube oriented grains. The purpose is to detect the influence of activation of non-octahedral slip systems and the role of strain rate sensitivity on Cube texture stabilization.

C. Texture Evolution During Hot Rolling: Crystal Plasticity Simulations

The activation of non-octahedral slip systems (i.e. $\{110\} \langle 110 \rangle$) at temperatures above 300 °C and their importance in good prediction of texture during hot rolling was already assessed.[38] The parameter r^{110} is used to quantify the activity of these slip systems and it is defined as:

$$r^{110} = \frac{\tau^{\{110\}}}{\tau^{\{111\}}} \qquad [9]$$

where $\tau^{\{110\}}$ is the critical resolved shear stress on non-octahedral slip systems and $\tau^{\{111\}}$ is the critical resolved shear stress on octahedral slip systems (i.e. $\{111\}\langle 110 \rangle$). This ratio of critical resolved shear stresses is related to the hot rolling temperature and strain rate through the Zener parameter. Given a constant strain rate, decreasing r^{110} corresponds to an increase of hot rolling temperature and more favored activation of non-octahedral slip systems. In the present simulations,

Table VI. Parameters of the Phenopower Law Used in DAMASK for Hot Rolling Simulations

Parameter	$r^{110} = 0.7$		$r^{110} = 1.0$		$r^{110} = 1.3$	
Slip System	Oct.	Non-oct.	Oct.	Non-oct.	Oct.	Non-oct.
# of Slip Systems	12	6	12	6	12	6
C11 [GPa]	106.75					
C12 [GPa]	60.41					
C44 [GPa]	28.34					
$\dot{\gamma}_0 [\text{s}^{-1}]$	0.001					
1/m	5, 40					
τ_c^β [MPa]	15.5	10.85	15.5	15.5	15.5	20.15
τ_s [MPa]	31.5	22.05	31.5	31.5	31.5	40.95
a	2.25					
$h0$ [MPa]	75					
$q_{\alpha\beta}$ (Self and Coplanar Slip Systems)	1.0					
$q_{\alpha\beta}$ (Non-coplanar slip systems)	1.4					

Table VII. Number of Rolling Passes Simulated in DAMASK for Hot Rolling of Al6016 With the F_{33} Value Implemented in the Simulation and the Corresponding Thickness Reduction

Rolling Pass	F_{33}	Thickness Reduction (Pct)	Total Thickness Reduction (Pct)
1st	0.67	33	33
2nd	0.82	18	45
3rd	0.82	18	55
4th	0.87	13	60.8
5th	0.87	13	65.9
6th	0.85	15	71
7th	0.85	15	75.4
8th	0.87	13	78.6
9th	0.87	13	81.4
10th	0.87	13	83.8
11th	0.87	13	85.9

values of 1.3, 1.0 and 0.7 were considered for r^{110}. Tables VI and VII show respectively the phenopower law values and the loading used in crystal plasticity simulations.

The influence of strain rate sensitivity on microstructure was simulated during hot rolling (plane strain compression) for an EBSD scan with the initial microstructure containing high Cube volume fraction for a value of m in the order of 10^{-2} (e.g. 0.025, thus between the cold-rolled values of 0.005 and 0.052) and the highest value of 0.2. The simulated rolling reduction was increased to 86 pct because, during hot rolling, depending on the starting slab thickness, the thickness reduction can be close to 90 pct or even higher. Cold rolling simulations were also repeated for these m values (0.025 and 0.2) and the same initial microstructure. The results were compared with variation of strain rate sensitivity during hot rolling. Figure 15(a) shows the evolution of Cube volume fraction versus thickness reduction for different strain rate sensitivities for cold and hot rolling. During hot rolling, it is confirmed that high values of m stabilize Cube. However, the curves shift to higher percentage of retained Cube volume fraction because activation of non-octahedral slip systems further stabilizes Cube (for r^{110} values equal or higher than 1.0). The gap between the curve for an m of 0.2 and the curve for an m of 0.025 diminishes as r^{110} decreases. This means that the influence of strain rate sensitivity on Cube texture evolution is more pronounced during hot rolling at temperatures lower than 500 °C or during cold rolling. In Figure 15(b), during hot rolling, Brass is not affected by the strain rate sensitivity value, because its volume fraction remains below 1 pct when activation of non-octahedral slip systems is favored (i.e. r^{110} equal to 1.0 or 0.7). As shown in Figure 15(c), during hot rolling as in cold rolling, a higher volume fraction of Copper is developed for an m of 0.2 than for lower values of m. For an m of 0.2, the activation of non-octahedral slip systems does not affect Copper, while for an m value of 0.025, the Copper fraction is higher when octahedral slip systems are easily activated (r^{110} of 1.0 and 0.7). S texture does
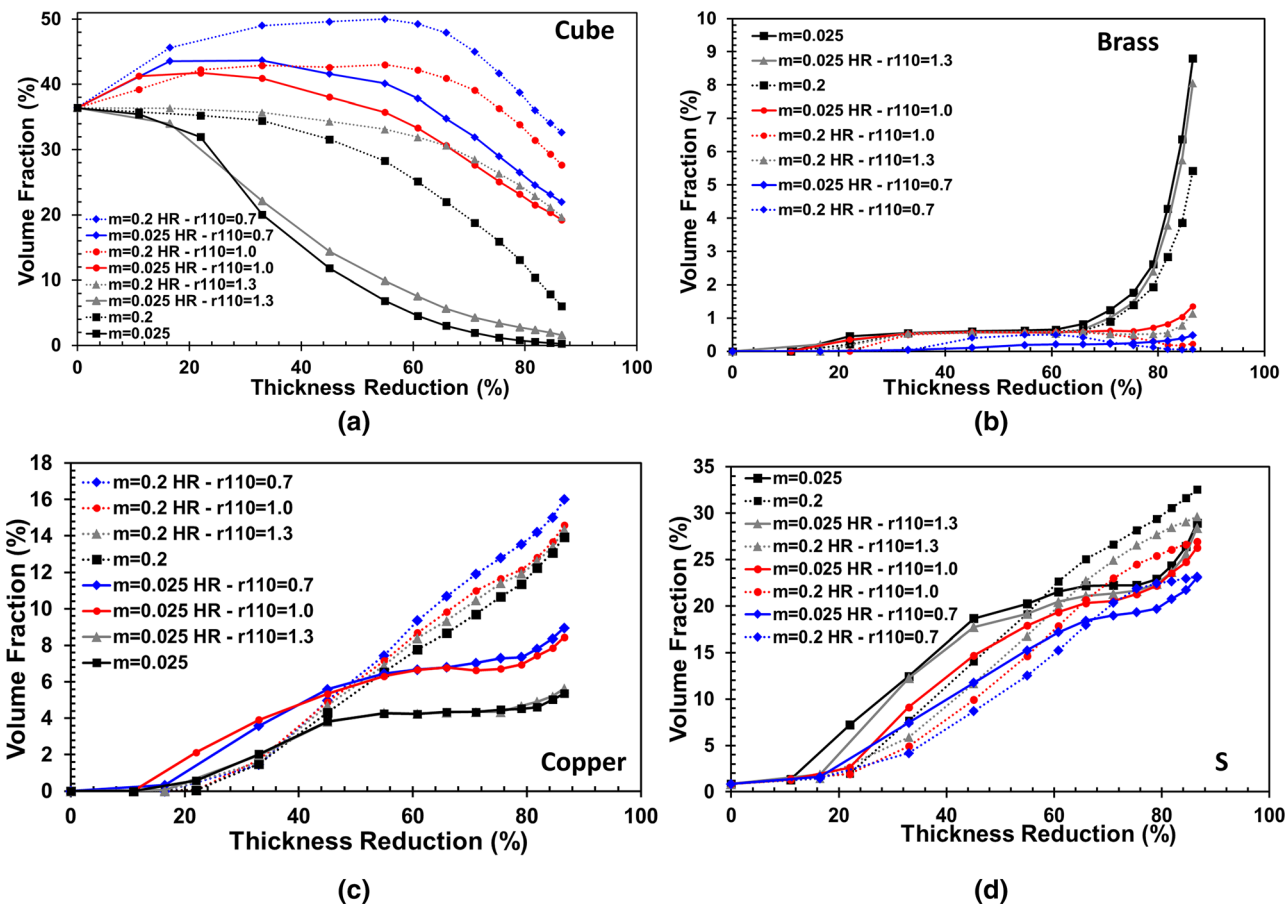
Fig. 15—Volume fraction as function of thickness reduction and strain rate sensitivity for several texture components (Cube (*a*), Brass (*b*), Copper (*c*) and S (*d*)) during hot rolling. Evolution extracted from crystal plasticity simulations.

not depend on strain rate sensitivity but activation of non-octahedral slip systems lowers the final amount of S texture in the microstructure (Figure 15(d)). According to Leffers,[10] high stacking fault energy and high rolling temperature would favor formation of Copper texture, while low rolling temperature and stacking fault energy would favor Brass formation. Compared to other FCC metals, the stacking fault energy of pure aluminium is 162 mJ/m^2 against 130 mJ/m^2 for nickel and 78 mJ/m^2 for Copper,[36] and this would be a factor promoting cross-slip and development of Copper texture at the expense of Brass texture.[10,11] Alloy composition affects stacking fault energy and in aluminium alloys hot rolling experiments have shown that the microstructure is Brass and Cube dominated in hot rolling,[39,40] because strong Brass texture is developed and Cube is stabilized. Vatne *et al.*[41] confirmed Cube stabilization through hot plane strain compression tests on AA 3004 for several values of temperature and strain rate using a recrystallized starting microstructure with 10 pct of Cube volume fraction. From this microstructure, Vatne[41] confirmed that for low values of r^{110} a stronger Brass component is produced. Cube stabilization during hot rolling is confirmed by crystal plasticity simulations in Figure 15(a), while the fraction of Brass is lower during hot rolling than cold rolling (Figure 15(b)) and

this result contradicts literature. Nevertheless, Maurice and Driver[39] performed hot rolling on a 3104 aluminium alloy with an initial microstructure having no Cube but only a random texture with very weak Brass, while Contrepois *et al.*[40] analyzed texture evolution during hot rolling of AA 2050 and AA 7050 with an initial texture characterized by S and Brass and with only 2 to 4 pct of Cube. Both these microstructures differ from the initial microstructure used in the crystal plasticity simulations presented here, where no initial Brass, S or Copper are present, but there is only 36 pct of Cube and 16 pct of Q texture, while the remaining are random orientations and this could explain while in these simulations the final microstructure contains more Copper and S than Brass for higher hot rolling temperatures. However, as discussed for cold rolling simulations, the choice of a 2D or 3D RVE also has an influence on Brass volume fraction. This was assessed for an r^{110} of 0.7 and the results are included in Appendix A in Figure A.1(d). More Brass is developed in a 3D RVE, but its volume fraction still remains lower than Copper and S. These simulations seem to suggest that initial microstructures containing more than 30 pct of Cube seem to promote more Copper and S than Brass during hot rolling.

In Figure 16, the value of strain rate sensitivity has no influence on Goss evolution during hot rolling, except
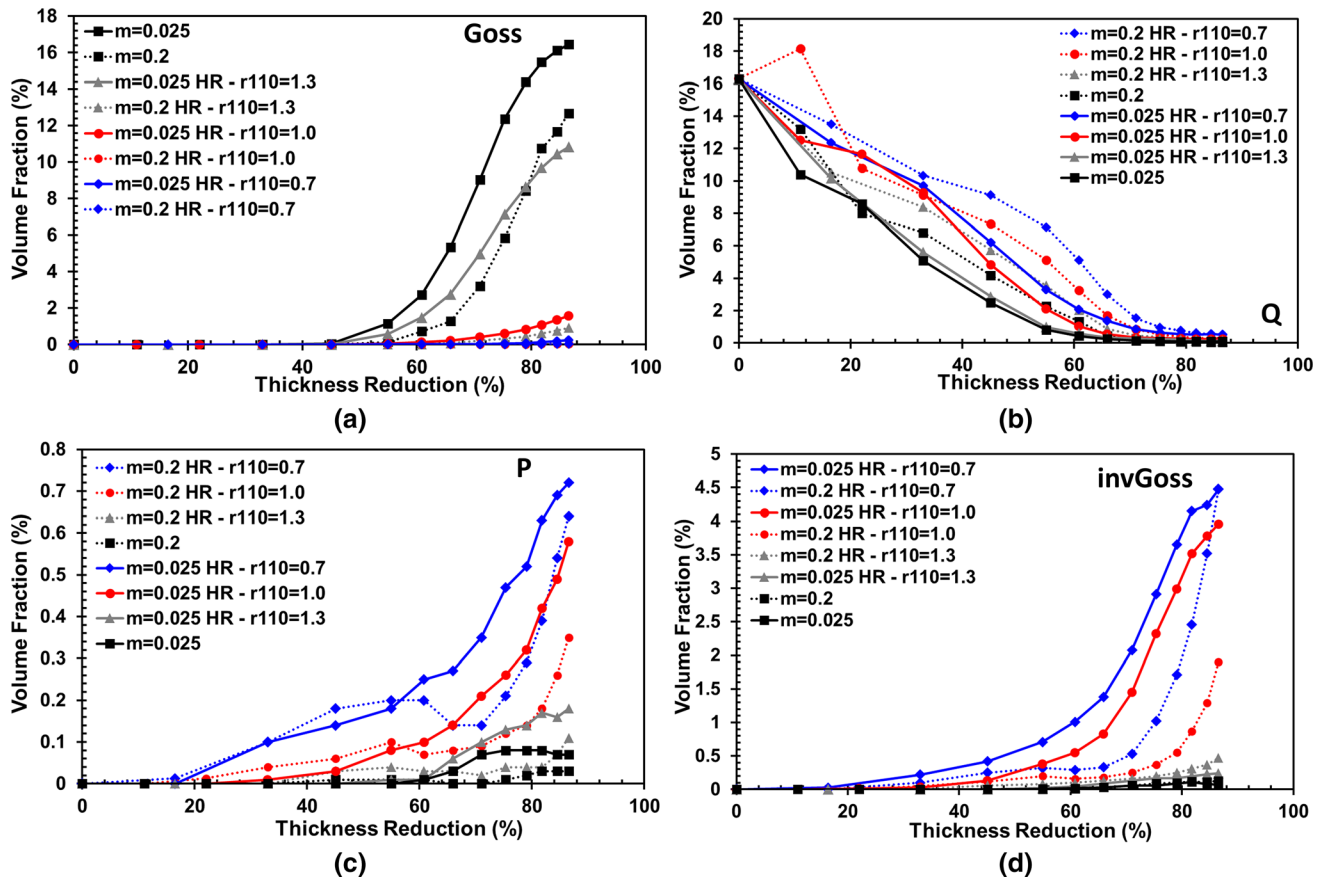
Fig. 16—Volume fraction as function of thickness reduction and strain rate sensitivity for several texture components (Goss (*a*), Q (*b*), P (*c*) and invGoss (*d*)) during hot rolling. Evolution extracted from crystal plasticity simulations.
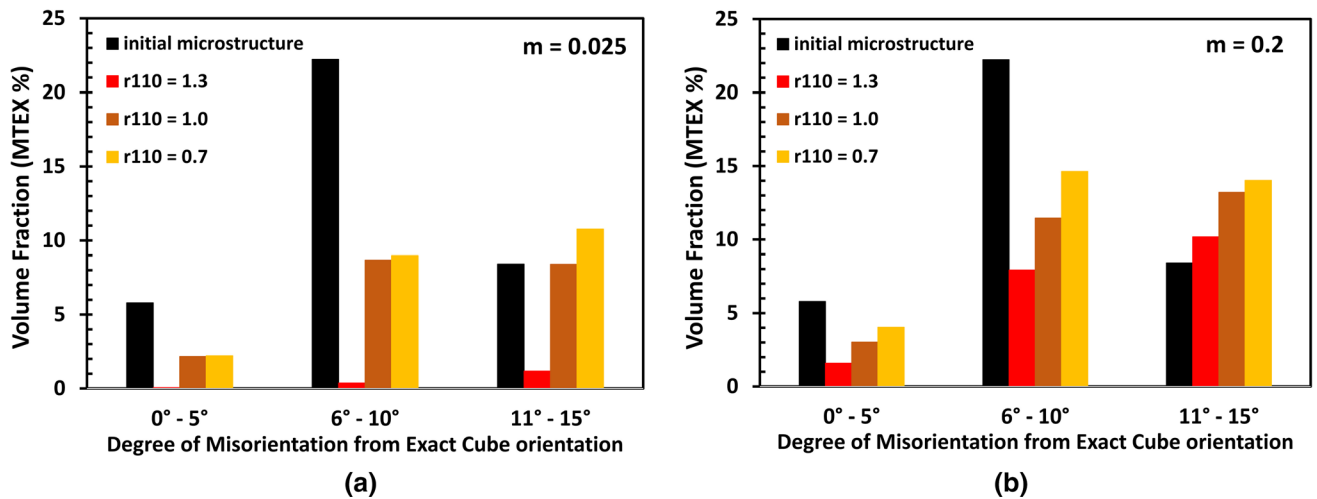

Fig. 17—Comparison of Cube fraction as function of its misorientation from exact Cube orientation extracted from crystal plasticity hot rolling simulations for different values of non-octahedral slip systems activation (*i.e.* different r^{110} values) and 0.025 and 0.2 strain rate sensitivities.

for an r^{110} of 1.3. At thickness reductions higher than 60 pct, Q texture evolution does not depend on r^{110} and m (Figure 16(b)). The volume fraction of P remains always lower than 1 pct (Figure 16(c)), while significant invGoss does not develop during cold rolling but only in hot rolling for r^{110} equal to 1.0 or 0.7 (Figure 16(d)).

Figure 17 shows the distribution of Cube volume fraction as function of its degree of misorientation for different r^{110} and *m* values for 83 pct thickness reduction. For *m* 0.025 and an r^{110} of 1.3, no volume fraction of Cube with 0 to 5 deg misorientation is preserved but all the Cube has between 10 and 15 deg misorientation
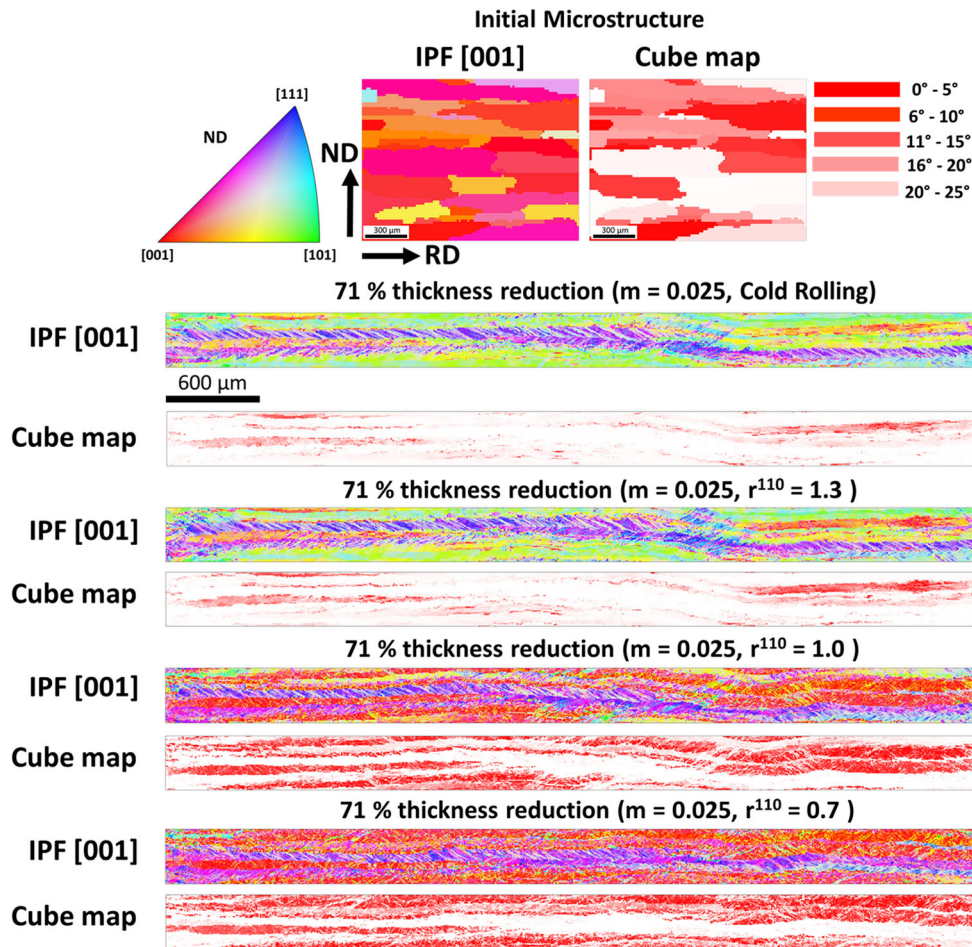
Fig. 18—Evolution of microstructure from crystal plasticity simulations in the RD-ND section for a strain rate sensitivity of 0.025 and several hot rolling conditions. Images show microstructures (IPF for normal direction (ND) and distribution of Cube grains) at 71 pct thickness reduction.

(Figure 17(a)). For easier activation of non-octahedral slip systems (r^{110} of 1.0 and 0.7) and for m values of 10^{-1}, more Cube is stabilized in the range 0 to 5 deg misorientation and in the range 6 to 15 deg misorientation (Figures 17(b)). Figures 18 and 19 show the RD-ND sections of the simulated microstructure for different values of r^{110} and the two values of strain rate sensitivity.

V. CONCLUSIONS

In texture simulations, the strain rate sensitivity value is often neglected or kept constant both for hot and cold rolling. The results presented here from crystal plasticity simulations highlight the importance of using the right strain rate sensitivity in texture prediction because this parameter influences the development of different texture components. Among all rolling texture components (*i.e.* Cube, Brass, Goss, S and Copper), Cube and Copper are the orientations most affected by changes in strain rate sensitivity values (*m*). Experimental rolling

textures from Al 6016 confirm stabilization of Cube texture at higher rolling speeds and a delay of its fragmentation resulting in a higher volume fraction of Cube preserving a misorientation lower than 15 deg from the exact Cube orientation. This stabilization is confirmed by a higher intensity for Cube texture in the ODF of specimens rolled at 600 m/min than sheets rolled at 80 m/min. For cold rolling:

- a high value of *m* will promote Cube stabilization and delay its fragmentation. This is observed for *m* values above or equal to 10^{-2} or for *m* values below 10^{-2} and thickness reductions lower than 70 pct;
- Copper volume fraction increases with strain rate sensitivity;
- Brass and S texture components are moderately affected by strain rate sensitivity;
- Goss volume fraction is low only if strain rate sensitivity is equal or higher than 0.2;
- Q, P and invGoss orientations are not affected by strain rate sensitivity.
- From analyses of RD-ND sections, high values of *m* seem to promote transition bands formation aligned
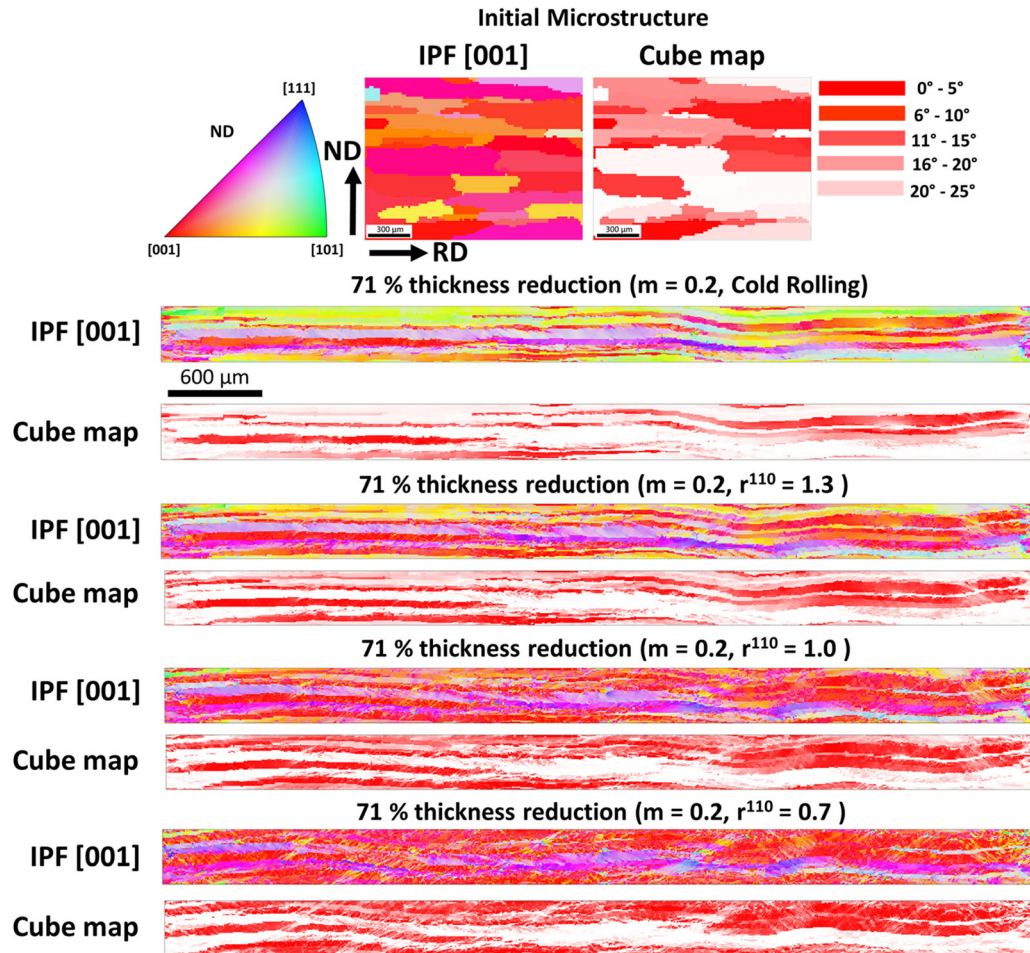
Fig. 19—Evolution of microstructure from crystal plasticity simulations in the RD-ND section for a strain rate sensitivity of 0.2 and several hot rolling conditions. Images show microstructures (IPF for normal direction (ND) and distribution of Cube grains) at 71 pct thickness reduction.

along RD. It is thus expected that aluminium alloys that show high values of strain rate sensitivity could be more prone to formation of transition bands which are preserved at thickness reduction equal or higher than 73 pct.

For hot rolling:

- Cube and Copper textures components are influenced by strain rate sensitivity more than other crystallographic orientations.

Furthermore, these results show that crystal plasticity simulations capture the influence of variations of strain rate sensitivity on texture evolution, however, the total amount of Cube is underestimated. Results of further crystal plasticity simulations show that the total fraction of Cube is affected by the choice of latent hardening and the selection of a 2D or 3D RVE. In cold rolling, for low strain rate sensitivities and thickness reductions below 80 pct, a 3D RVE stabilizes 2 to 3 pct more Cube. In hot rolling, a higher amount of Cube is predicted for a 2D RVE than a 3D RVE even at reductions higher than 80 pct. However, the tendencies of Cube fraction evolution as function of strain rate sensitivity are the same both for 2D and 3D RVEs. The total amount of Brass is better estimated in 3D RVEs because the F_{12} is macroscopically zero, but locally can be non-zero. Nevertheless, 2D RVEs have the advantage that EBSD microstructures can be directly imported for crystal plasticity simulations and this ensures that the initial texture distribution, the grain boundary shape and the distribution of grains orientation and size is fully representative of the measurement in the RD-ND plane.

AUTHOR CONTRIBUTIONS

EC: Conceptualization, Methodology, Investigation, Formal analysis, Visualization, Writing-original draft, Writing-review and editing. GF: Writing-review and editing, Funding acquisition, Resources. SM: Investigation, Writing-review and editing. MT: Investigation, Writing-review and editing. SK: Investigation, Writing-review and editing. FR: Resources, Writing-review and editing, Supervision, Funding acquisition.

CONFLICT OF INTEREST

The authors declare that they have no known competing financial interests or personal relationships that could have appeared to influence the work reported in this paper.

DATA AVAILABILITY

All data that support the findings of this study are within the article.

APPENDIX A: TEXTURE EVOLUTION AS FUNCTION OF M: COMPARISON BETWEEN 2D AND 3D RVE

Further crystal plasticity simulations were performed to compare the selection of a starting 2D or 3D RVE on texture evolution. In 3D RVEs, artificial microstructures must be created and the grain boundary shape in the third dimension, the distribution of grains orientations and size might not be completely representative of the real specimen. Another part of the analysis was done reducing the number of remeshing steps to highlight possible influence of remeshing on texture development when a thickness reduction of 87 pct has to be obtained. Thus, the EBSD orientations employed in hot rolling simulations were used for texture simulations under plane strain compression in a 3D RVE with 43 starting grains elongated in RD direction and with an initial grid of $24 \times 24 \times 24$ voxels. Crystal plasticity cold rolling simulations were performed by applying the same number of remeshing steps (*i.e.* ten) used for the 2D-RVE during hot rolling and cold rolling shown in section 4.3 and the m values of 0.025 and 0.2 were considered. The comparison between 2D and 3D RVEs was performed also in hot rolling conditions for strong activation of non-octahedral slip systems (r^{110} of 0.7). Figures A.1(a), (b), (c) and (d) show the comparison of texture evolution for 2D and 3D RVEs for Cube and Brass. 3D RVE stabilizes 2 to 3 pct more Cube compared to 2D RVE for a strain rate sensitivity of 0.025, while for an m of 0.2, more Cube is stabilized in the 2D RVE (Figure A.1(a)). This difference cancels out when the thickness reduction is above 70 pct. Moreover, the dependence of Cube volume fraction on strain rate sensitivity is the same both for 2D and 3D RVEs (*i.e.* more Cube is stabilized for high values of strain rate sensitivity). For hot rolling, the Cube volume fraction is more stabilized if a 2D RVE is considered, but for both RVEs, the Cube fraction is higher if the strain rate sensitivity is 0.2 (Figure A.1(b)). For Brass (Figures A.1(c) and A.1(d)), the dependence of volume fraction on strain rate sensitivity is the same for both RVEs, but as thickness reduction increases, a higher Brass volume fraction is found in 3D RVE.

The evolution of Copper as function of strain rate sensitivity is affected by the choice of 2D or 3D RVE. Figure A.2(a) shows that for a 2D RVE, a higher volume fraction is obtained for an m of 0.2 than an m of 0.025 (which is the trend confirmed by samples rolled at different speeds); while, a 3D RVE does not capture a dependence of the volume fraction on strain rate sensitivity. For Copper, this discrepancy between 2D and 3D RVEs is present also in hot rolling (Figure A.2(b)) and the reason would require more analyses as it was not reported in literature before and it is not clear if this could be due to F_{12} being non-zero locally in the 3D RVE. S texture is less affected by a 2D or 3D RVEs choice compared to Copper, however 8 pct more volume fraction is obtained for a 3D RVE when m is 0.025 both in cold (Figure A.2(c)) and hot (Figure A.2(d)) rolling.

Increase of Goss volume fraction in cold rolling is delayed for 2D RVEs while for both RVEs a higher Goss fraction is obtained for an m of 0.025 than for 0.2 (Figure A.3(a)). During hot rolling, the dependence of Goss on strain rate sensitivity does not depend on the choice of the RVE, but a higher volume fraction is found in the 3D RVE even if the difference is just 1 pct (Figure A.3(b)). The Q texture component is not affected by 2D or 3D RVEs (Figures A.3(c) and (d)). The same was found for P and invGoss textures components whose variations are in the range of 0.1 to 0.2 pct and thus were not added in the graphs.
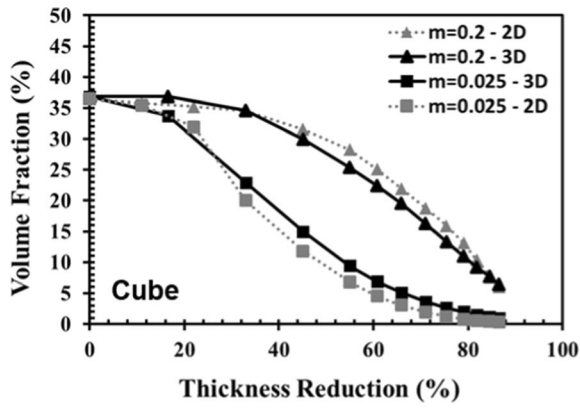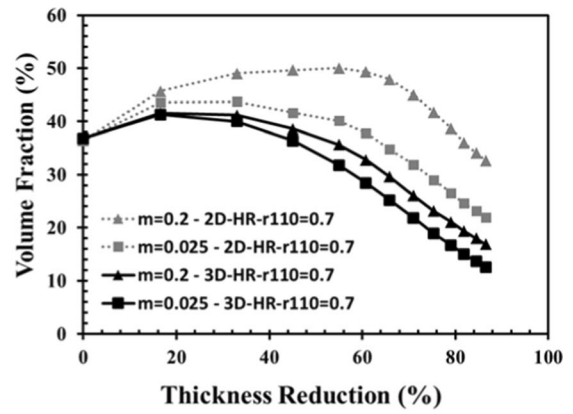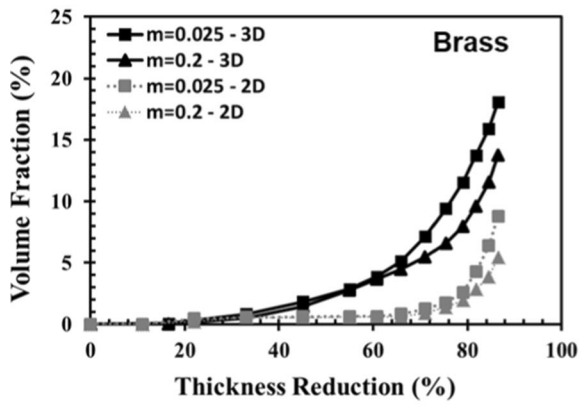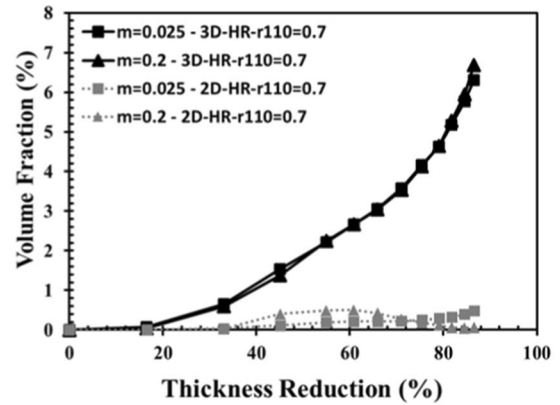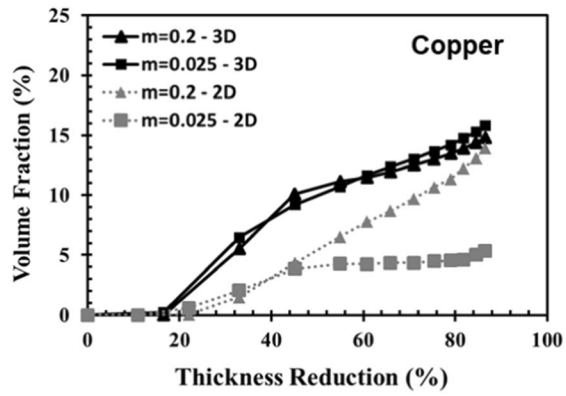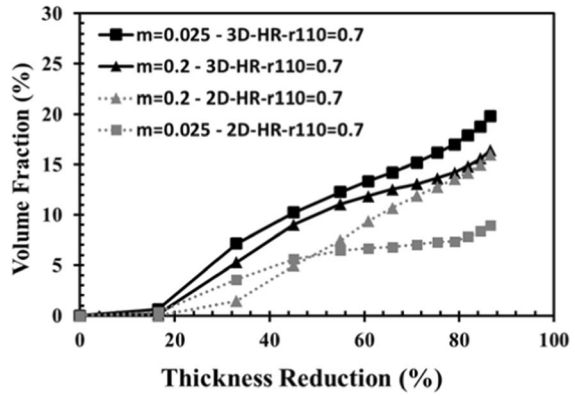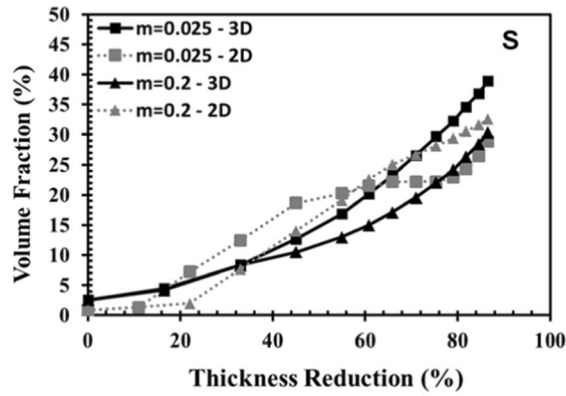
Fig. A.1—Comparison of Cube ((*a*) and (*b*)) and Brass ((*c*) and (*d*)) texture evolution for 2D and 3D RVEs during cold and hot rolling (HR) for two different strain rate sensitivity values (*i.e.* 0.025 and 0.2).
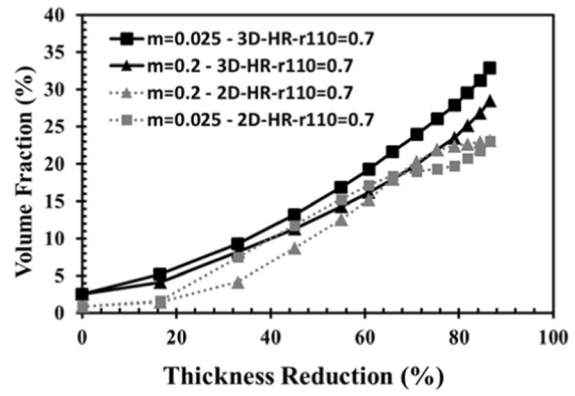
Fig. A.2—Comparison of Copper ((*a*) and (*b*)) and S ((*c*) and (*d*)) texture evolution for 2D and 3D RVEs during cold and hot rolling (HR) for two different strain rate sensitivity values (*i.e.* 0.025 and 0.2)..
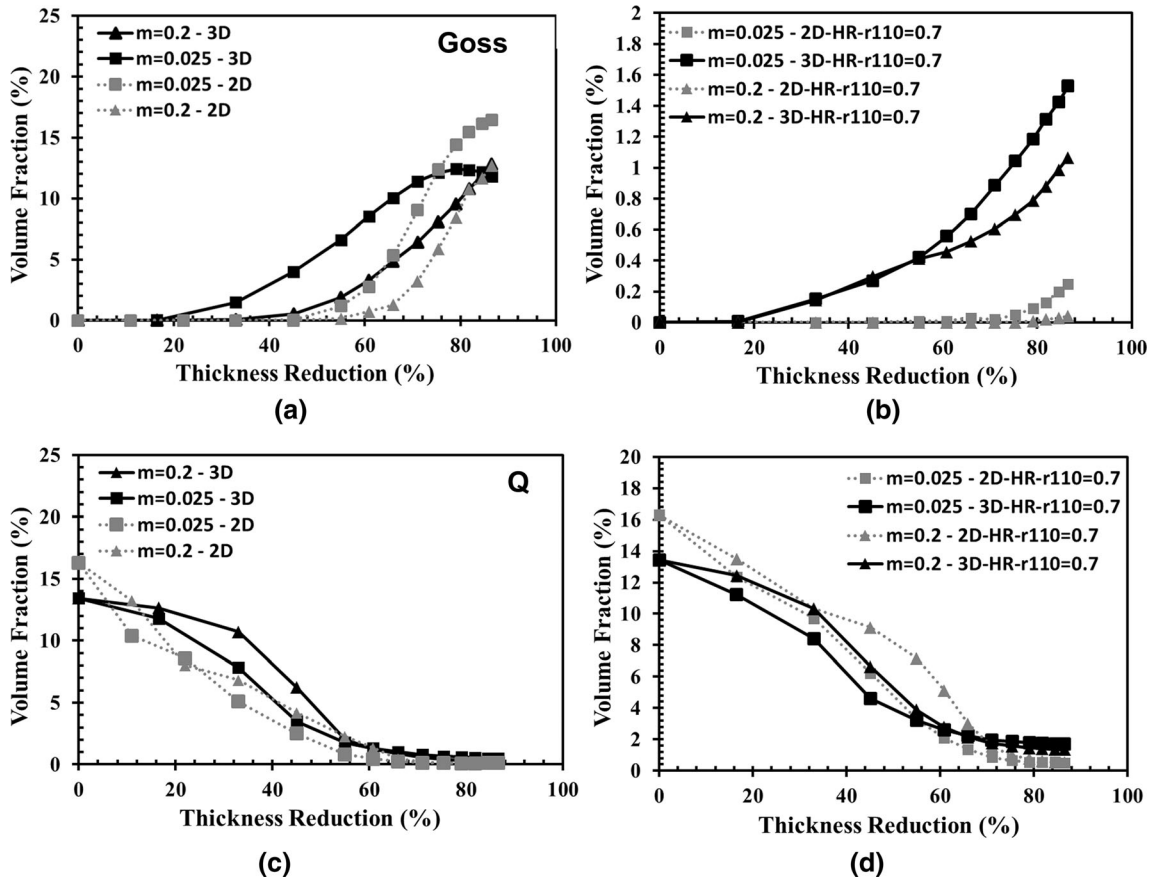
Fig. A.3—Comparison of Goss ((*a*) and (*b*)), and Q ((*c*) and (*d*)) texture evolution for 2D and 3D RVEs during cold and hot rolling (HR) for two different strain rate sensitivity values (*i.e.* 0.025 and 0.2).

APPENDIX B: TEXTURE EVOLUTION AS FUNCTION OF *M*: CHANGE OF NUMBER OF REMESHING STEPS

Another set of simulations for the 3D-RVE was performed by reducing the number of remeshing steps and performing remeshing only four times to complete the full 87 pct thickness reduction. For both simulations, only the *m* values of 0.025 and 0.2 were considered during cold rolling.

Figure B.1 compares texture evolution for different number of remeshing steps. Cube, Brass, Copper, S,

Goss and Q orientations are not affected by a change in number of remeshing steps. Little differences (0.1 pct) are found for P and invGoss textures. Moreover, when a remeshing step is performed on the microstructure of the RVE, the volume fraction of texture components as well as orientations distribution are controlled before and after remeshing to ensure that remeshing is fine enough to avoid disappearance of texture components.
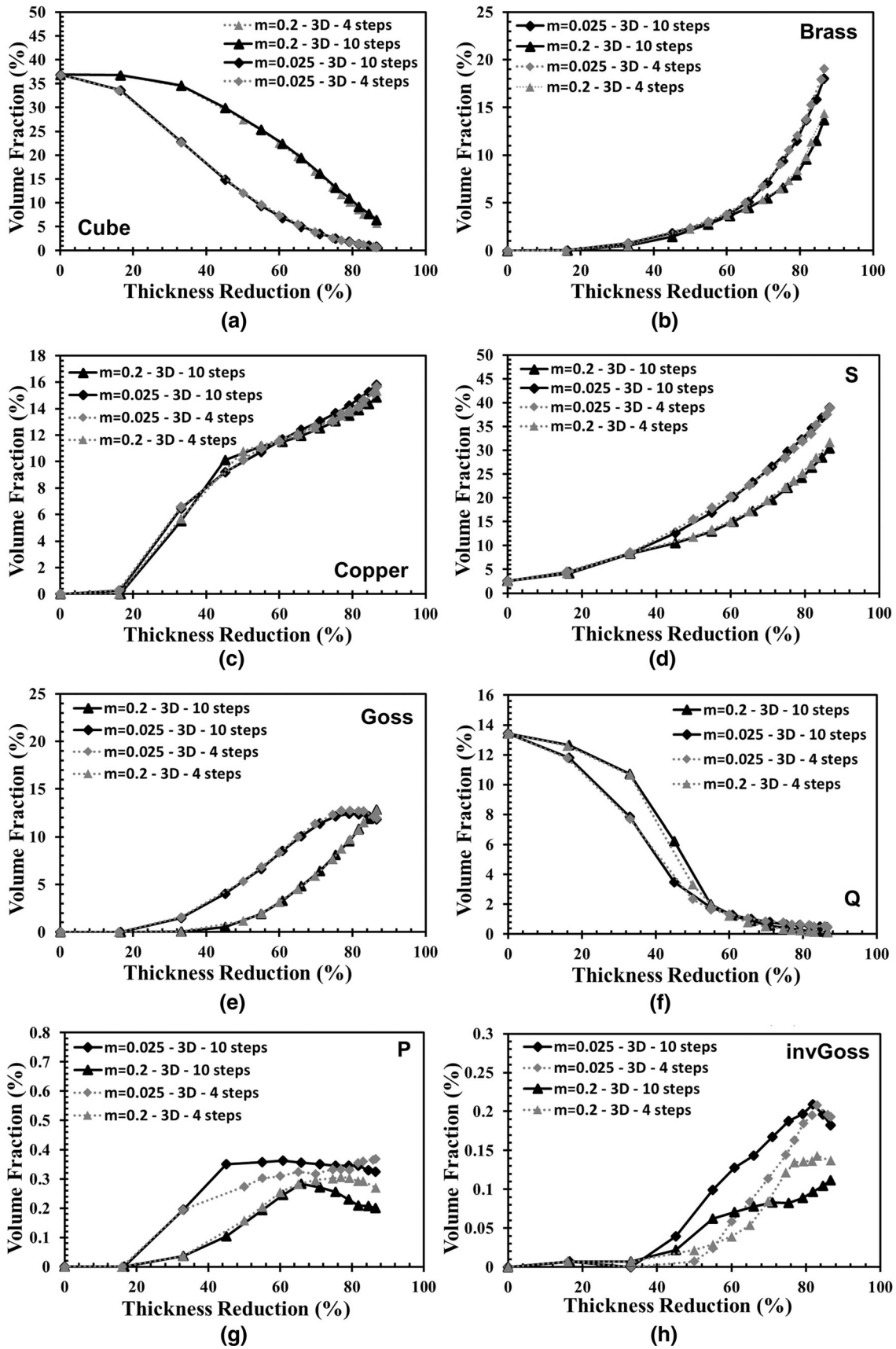
Fig. B.1—Comparison of texture evolution for 3D RVEs during cold rolling for different number of remeshing steps and strain rate sensitivity values (*i.e.* 0.025 and 0.2) ((*a*) through (*h*)).

APPENDIX C. TEXTURE EVOLUTION
AS FUNCTION OF LATENT HARDENING

Figure C.1 shows the influence of latent hardening variations on texture evolution for the most important texture components.
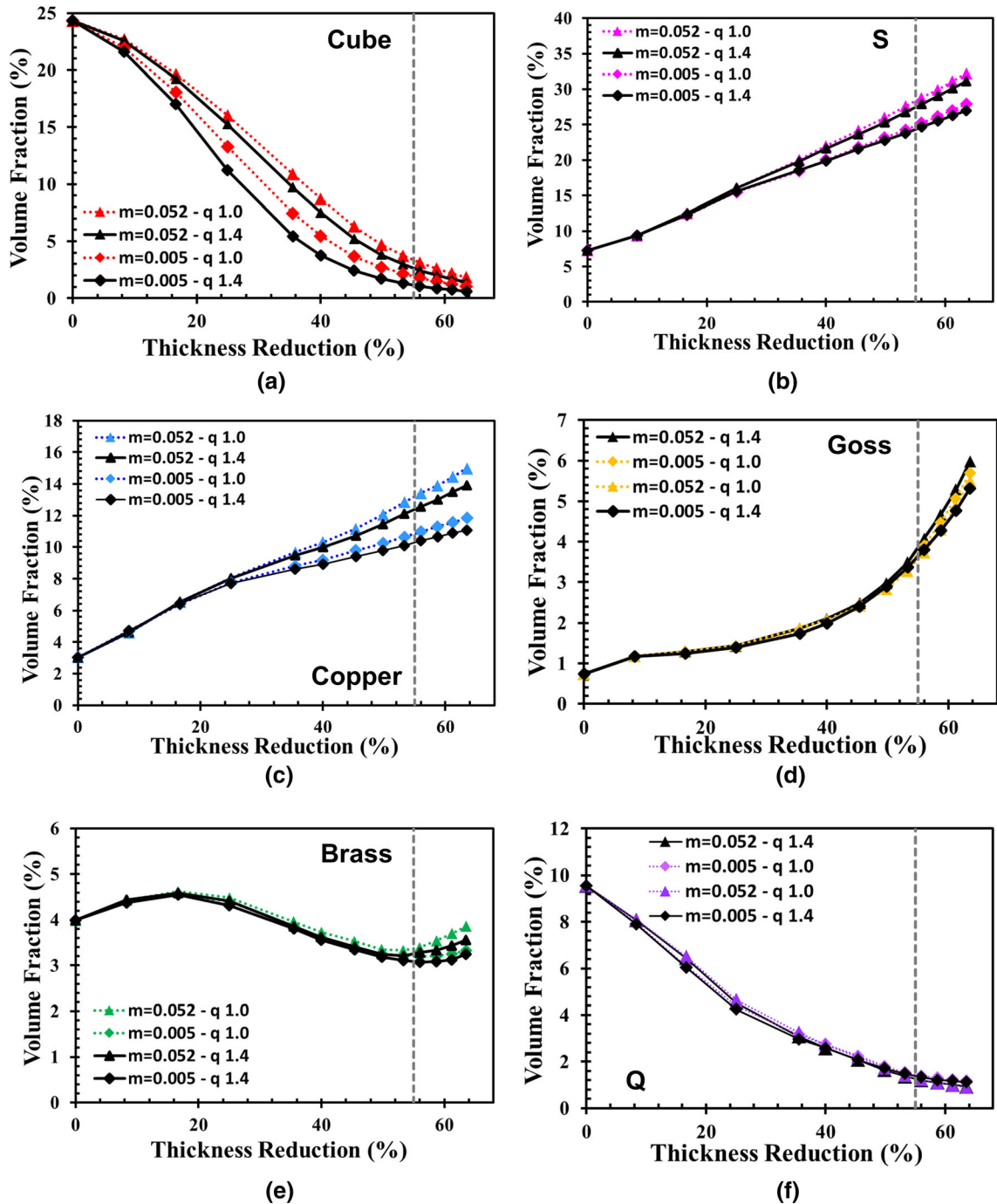

Fig. C.1—Evolution of several texture components ((*a*) through (*f*)) as function of thickness reduction for an initial microstructure of 2850 μm $\times$ 2260 μm considering different latent hardening (dashed curve corresponds to 55 pct thickness reduction).

REFERENCES

1. A. Chapuis and Q. Liu: *Int. J. Solids Struct.*, 2018, vol. 152–153, pp. 217–27.
2. F. Montheillet and J.J. Jonas: *Metall. Mater. Tras. A*, 1996, pp. 3346–48.
3. O.G. Lademo, O. Engler, J. Aegerter, T. Berstad, A. Benallal, and O.S. Hopperstad: *J. Eng. Mater. Technol. Trans. ASME*, 2010, vol. 132, pp. 1–8.
4. R.C. Picu, G. Vincze, J.J. Gracio, and F. Barlat: *Scr. Mater.*, 2006, vol. 54, pp. 71–75.
5. E. Romhanji, M. Dudukovska, and D. Gliši: *J. Mater. Process. Technol.*, 2002, vol. 125–126, pp. 193–238.
6. A.Y. Ku, A.S. Khan, and T. Gnäupel-Herold: *Int. J. Plast.*, DOI:https://doi.org/10.1016/j.ijplas.2020.102679.
7. S.S.L. Vendra, S. Goel, N. Kumar, and R. Jayaganthan: *Mater. Sci. Eng. A*, 2017, vol. 686, pp. 82–92.
8. A. Vevecka-Priftaj, A. Böhner, J. May, H.W. Höppel, and M. Göken: *Mater. Sci. Forum*, 2008, vol. 584-586 PA, pp. 741–47.
9. J. Hirsch: *Mater. Sci. Forum*, 2008, vol. 604–605, pp. 259–66.
10. T. Leffers: *Scr. Metall.*, 1968, vol. 2, pp. 447–52.
11. T. Leffers and O.B. Pedersen: *Scr. Mater.*, 2002, vol. 46, pp. 741–46.
12. O. Engler, P. Wagner, J. Savoie, D. Ponge, and G. Gottstein: *Scr. Metall. Mater.*, 1993, vol. 28, pp. 1317–22.
13. R.J. Asaro and A. Needleman: *Acta Metall.*, 1985, vol. 33, pp. 923–53.
14. S. Panchanadeeswaran and D.P. Field: *Acta Metall. Mater.*, 1995, vol. 43, pp. 1683–92.
15. R.A. Lebensohn and C.N. Tomé: *Acta Metall. Mater.*, 1993, vol. 41, pp. 2611–24.
16. P. Van Houtte, S. Li, M. Seefeldt, and L. Delannay: *Int. J. Plast.*, 2005, vol. 21, pp. 589–624.
17. S.J. Hosseinipour: *Mater. Des.*, 2009, vol. 30, pp. 319–22.
18. L. Xin, L. Xiangping, and G. Changgang: in *2nd International Conference on High Speed Forming*, 2006, pp. 49–60.
19. O. Engler, J. Hirsch, K. Karhausen, and G. Gottstein: *Mater. Sci. Forum*, 1994, vol. 157–6, pp. 673–78.
20. N.K. Singh, M.K. Singha, E. Cadoni, and N.K. Gupta: *Adv. Mater. Res.*, 2012, vol. 548, pp. 169–73.
21. L. Djapic Oosterkamp, A. Ivankovic, and G. Venizelos: *Mater. Sci. Eng. A*, 2000, vol. 278, pp. 225–35.
22. A.S. Khan, J. Liu, J.W. Yoon, and R. Nambori: *Int. J. Plast.*, 2015, vol. 67, pp. 39–52.
23. J.K. Holmen, B.H. Frodal, O.S. Hopperstad, and T. Børvik: *Int. J. Plast.*, 2017, vol. 99, pp. 144–61.
24. S.L. Yan, H. Yang, H.W. Li, and X. Yao: *J. Alloys Compd.*, 2016, vol. 688, pp. 776–86.
25. ISO 26203-2: 2011.
26. W. Boehme: *FAT-Richtlinie 'Dynamische Werkstoffkennwerte Fuer Die Crashsimulation,'* Carl Hanser Verlag, Muenchen, 2008.
27. Z. Jia, B. Guan, Y. Zang, Y. Wang, and L. Mu: *Mater. Sci. Eng. A*, 2021, vol. 820, 141565.
28. F. Roters, M. Diehl, P. Shanthraj, P. Eisenlohr, C. Reuber, S.L. Wong, T. Maiti, A. Ebrahimi, T. Hochrainer, H.O. Fabritius, S. Nikolov, M. Friák, N. Fujita, N. Grilli, K.G.F. Janssens, N. Jia, P.J.J. Kok, D. Ma, F. Meier, E. Werner, M. Stricker, D. Weygand, and D. Raabe: *Comput. Mater. Sci.*, 2019, vol. 158, pp. 420–78.
29. M.A. Groeber and M.A. Jackson: *Integr. Mater. Manuf. Innov.*, 2014, vol. 3, pp. 56–72.
30. M. Kasemer, G. Falkinger, and F. Roters: *Modelling Simul. Mater. Sci. Eng.*, 2020, vol. 28, art. no. 085005.
31. F. Roters, P. Eisenlohr, L. Hantcherli, D.D. Tjahjanto, T.R. Bieler, and D. Raabe: *Acta Mater.*, 2010, vol. 58, pp. 1152–1211.
32. U.F. Kocks: Metall. *Mater. Trans.*, 1970, vol. 1, pp. 1121–43.
33. D. Peirce, R.J. Asaro, and A. Needleman: *Acta Metall.*, 1982, vol. 30, pp. 1087–1119.
34. K. Sedighiani, V. Shah, K. Traka, M. Diehl, F. Roters, J. Sietsma, and D. Raabe: *Int. J. Plast.*, 2021, vol. 146, 103078.
35. G.R. Canova, C. Fressengeas, A. Molinari, and U.F. Kocks: *Acta Metall.*, 1988, vol. 36, pp. 1961–70.
36. N.P. Gurao, R. Kapoor, and S. Suwas: *Metall. Mater. Trans. A Phys. Metall. Mater. Sci.*, 2010, vol. 41, pp. 2794–2804.
37. B. Hum, H.W. Colquhoun, and J.G. Lenard: *J. Mater. Process. Technol.*, 1996, vol. 60, pp. 331–38.
38. J. Driver, F. Perocheau, and C. Maurice: *Mater. Sci. Forum*, 2000, vol. 331, pp. 43–56.
39. C. Maurice and J.H. Driver: *Mater. Sci. Forum*, 1994, vol. 157–6, pp. 807–12.
40. Q. Contrepois, C. Maurice, and J.H. Driver: *Mater. Sci. Eng. A*, 2010, vol. 527, pp. 7305–12.
41. H.E. Vatne, R. Shahani, and E. Nes: *Acta Mater.*, 1996, vol. 44, pp. 4447–62.